Legionella pneumophila modulates host cytoskeleton by an effector of transglutaminase activity

Yan Liu, Yao Liu[a], Zhao-Qing Luo[*]

Purdue Institute for Inflammation, Immunology and Infectious Diseases and Department of Biological Sciences, Purdue University, West Lafayette, IN, United States of America

*,Correspondence: luoz@purdue.edu

[a] Current address: PTC Therapeutics, 100 Corporate Ct #2400, South Plainfield, NJ 07080

Abstract

The bacterial pathogen *Legionella pneumophila* delivers more than 330 effector proteins into host cells through its Dot/Icm type IV secretion system (T4SS) to facilitate its intracellular replication. A number of these effectors modulate organelle trafficking pathways to create a membrane-bound niche called the *Legionella* containing vacuole (LCV). In this study, we found that *L. pneumophila* induces F-actin accumulation in host cell cortex by its Dot/Icm substrate RavJ (Lpg0944). RavJ harbors an $C_{101}H_{138}D_{170}$ motif associated with human tissue transglutaminases (TGs). We showed that RavJ catalyzes a covalent linkage between actin and the Motin family proteins Angiomotin (AMOT) and Angiomotin-like 1 (AMOTL1), proteins known to regulate tube formation and cell migration. Further study revealed that RavJ-induced crosslink between actin and AMOT occurs on its Gln_{354} residue. Crosslink between actin and AMOT significantly reduces the binding between actin and its binding partner cofilin, suggesting that RavJ inhibits actin depolymerization. We also demonstrated that the metaeffector LegL1 directly interacts with RavJ to antagonize its transglutaminase activity, leading to reduced crosslink between actin and Motin proteins. Our results reveal a novel mechanism of modulating the host actin cytoskeleton by *L. pneumophila*.

Introduction

Legionella pneumophila is a Gram-negative intracellular pathogen that causes Legionnaires' disease in humans[1]. Successful colonization by this bacteria requires its ability to manipulate such diverse processes of host cells as membrane trafficking, immunity, protein translation, autophagy, gene expression, and cytoskeleton structure[2, 3]. Upon entry into host cells, *L. pneumophila* promotes the biogenesis of a phagosome structure called the *Legionella*-containing vacuole (LCV) that supports its intracellular replication[4]. The virulence of *L. pneumophila* is correlated with its ability to survive and replicate in the LCV[4]. Biogenesis of the LCV requires the Dot/Icm system that transports over 330 protein substrates into the host cell[5, 6]. The activity of these effectors is essential for the development and maintenance of this replicative niche[4].

The actin cytoskeleton is involved in many essential cellular events such as mitosis, cell migration, control of epithelial barrier function, and adherence of immune cells[7]. Given the essential roles of the actin cytoskeleton, it is not surprising that this network is a common target for bacterial virulence factors[8]. *Yersinia* blocks macrophage phagocytosis by interfering with host Rho GTPase and the actin cytoskeleton dynamics[9]. *Salmonella enterica* Typhimurium delivers a subset of bacterial effector proteins into the eukaryotic host cell to modulate the host cell actin cytoskeleton, facilitating its own internalization into non-phagocytic cells[10]. *L. pneumophila* has also acquired the ability to modulate the actin cytoskeleton by its Dot/Icm substrates. For example, RavK is a protease that disrupts host cytoskeletal structure by cleaving actin[11]; LegK2 targets the actin nucleator ARP2/3 complex by phosphorylating its components ARPC1B and ARP3, leading to the global actin cytoskeleton remodeling in

cells[12]; Ceg14 affects actin distribution and inhibits actin polymerization by a yet unknown mechanism[13]; VipA interferes with organelle trafficking by acting as a nucleator for actin polymerization[14].

Post-translational modifications (PTMs) of host proteins involved in important cellular processes is a commonly used mechanism used by bacterial pathogens to counteract host defense[15]. PTMs often is executed by virulence factors that display diverse biochemical activities. A number of unique PTMs have been found to be imposed by Dot/Icm effectors, including phosphorylcholination[16, 17], AMPylation[18], phosphorylation[19], ADP-ribosylation[20-22], ubiquitination[20, 23], and transglutamination[23]. Among these, transglutamination is induced by transglutaminases (TGs) that primarily catalyze the formation of an isopeptide bond between the γ-carboxamide group of a glutamine residue from one protein and the ε-amino group of a lysine residue of another protein with the release of an ammonia[24]. This modification has been identified as an important PTM that attacks a wide spectrum of host functions to benefit the pathogens. For example, the HopX (AvrPphE) family of *Pseudomonas syringae* Type III effectors are composed of a conserved putative cysteine-base catalytic triad resemble of the transglutaminase family that is required for the generation of a cell-death response in specific *Arabidopsis* ecotypes[25]. The type III effector VopC promotes *Vibrio* invasion by activating Rac and CDC42 via its transglutaminase activity[26]. Modification by transglutamination by *L. pneumophila* effectors has recently emerged as an important virulence factor of this bacterium. The *L. pneumophila* effector MavC has been characterized as a transglutaminase that catalyzes

the formation of a covalent linkage between ubiquitin and UBE2N, leading to the inhibition of NF-κB signaling in the initial phase of bacterial infection[23].

Here, we showed that the Dot/Icm substrate RavJ (Lpg0944) catalyzes crosslink between actin and members of the Motin family, AMOT and AMOTL1, via its transglutaminase activity, leading to accumulation of actin polymers in mammalian cells. We also showed that the transglutaminase activity of RavJ is regulated by another Dot/Icm substrate LegL1(Lpg0945), which directly binds to RavJ and inhibits the enzymatic activity of RavJ.

Results

RavJ is a transglutaminase that induces actin accumulation in mammalian cells. RavJ was originally identified in a study aiming to analyze the mechanism of metaeffector activity in *L. pneumophila*[27]. Structural analysis reveals that RavJ harbors a C-H-D ($C_{101}H_{138}D_{170}$) motif associated with members of tissue transglutaminases (TGs)[27]. In a screening to identify Dot/Icm substrates capable of regulating the actin cytoskeleton, we transfected HEK293T cells with a GFP fusion library of Dot/Icm substrates and found that RavJ causes rearrangements of the actin cytoskeleton in mammalian cells (**Fig 1**). To determine the role of the putative catalytic motif potentially involved in TG activity in the function of RavJ, we introduced mutations in C_{101}, H_{138}, D_{170}, respectively, and found that each of these mutations completely abolished the ability of RavJ to induce actin cytoskeleton rearrangements (**Fig 1**). These results indicate that overexpression of RavJ triggers the formation of actin filaments in the cell cortex by a mechanism that requires its $C_{101}H_{138}D_{170}$ motif.

98

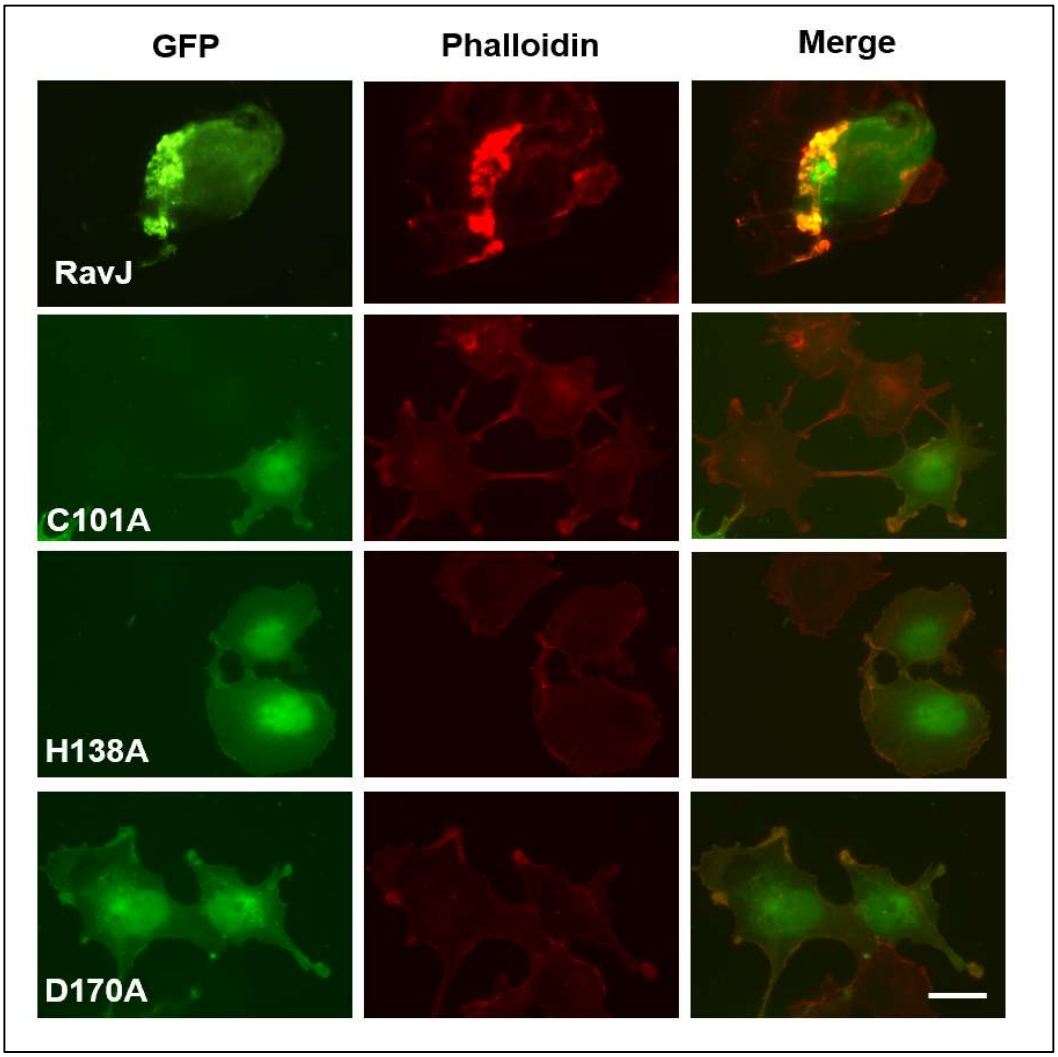

99

Fig 1. Ectopic expression of RavJ causes rearrangement of actin cytoskeleton. HEK293T cells were transfected with the indicated constructs and then subjected to immunofluorescence microscopic analysis. F-actin was stained by phalloidin conjugated with Texas-Red. Bar, 10 μm. Note that wild-type RavJ induces actin accumulation in the cell cortex and this phenotype is dependent on the predicted TG enzymatic motif.

ravJ* is dispensable for intracellular growth of *L. pneumophila

To examine the role of *ravJ* in *L. pneumophila* virulence, we first determined the level of RavJ at different growth phases throughout its growth cycle in broth. RavJ was detectable in all growth phases (optical density at 600 nm (OD_{600}) of 0.5-3.5) but became highly expressed in the lag phase (OD_{600}=0.5-0.7) (**Fig 2A**) after saturated cultures were diluted into fresh medium, suggesting that RavJ functions in the initial phase of infection.

We also determined the role of *ravJ* in *L. pneumophila* virulence by examining intracellular bacterial replication of relevant bacterial strains. The mutant Lp02Δ*ravJ* grew at rates indistinguishable from that of the wild-type strain (**Fig 2B-C**), indicating that, similar to most Dot/Icm substrates, RavJ is not required for proficient intracellular bacterial replication in commonly used tissue culture hosts.

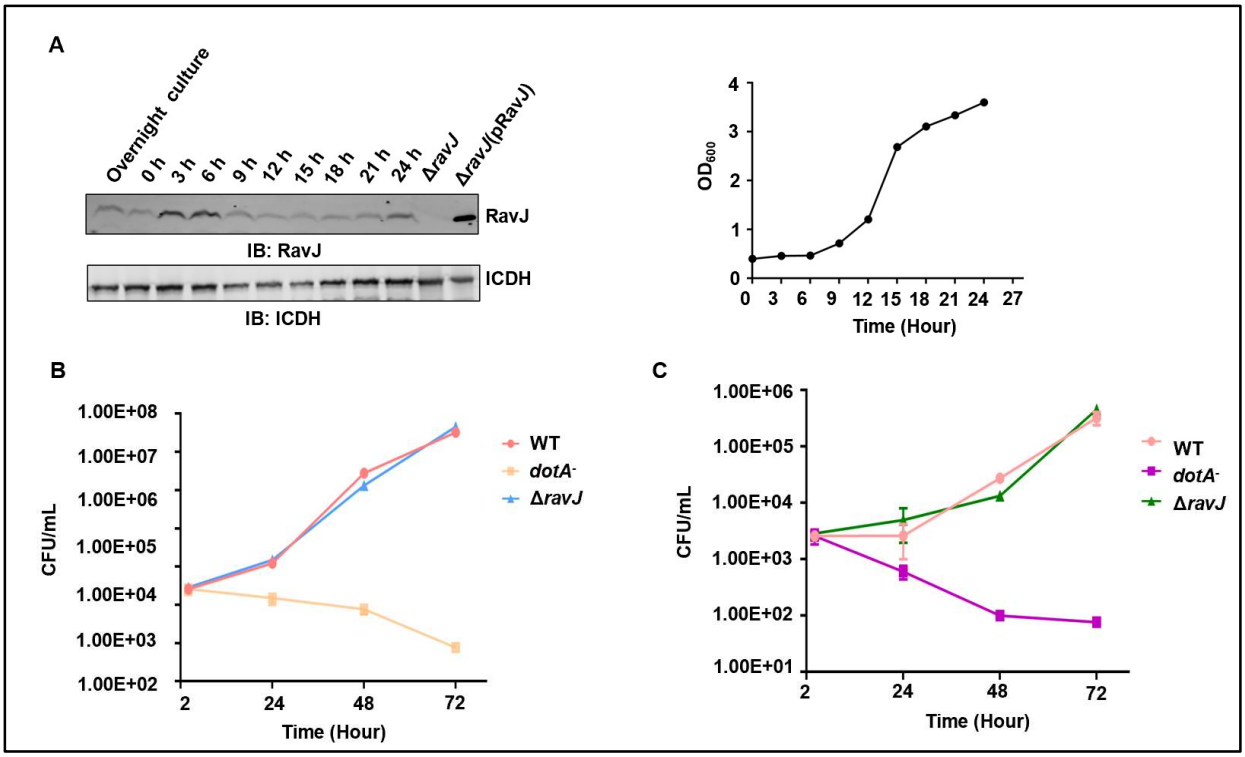

111

Fig 2. *ravJ* does not influence intracellular growth of *L. pneumophila*. **A**. The growth of *L. pneumophila* in AYE broth (right) and the expression of RavJ in bacteria grown in broth (left). Cultures grown to stationary phase were diluted 1:20 into fresh medium and the growth of bacteria was monitored by measuring OD_{600} at the indicated time points. **B-C**. The Δ*ravJ* strain grew at rates indistinguishable from that of the wild-type strain in commonly used tissue culture hosts. Bone marrow-derived mouse macrophages (BMDMs) **(B)** or *Dictyostelium discoideum* **(C)** were infected with relevant *L. pneumophila* strains at the indicated time points, cells were treated with 0.02% saponin for half an hour and the bacteria number was determined by enumerating colony-forming unit (CFU) of appropriately diluted lysates obtained by saponin. Errors bars represent ±SEM; n=3;

Ectopically expressed RavJ crosslinks with actin. TGs function to catalyze homo- or heterologous protein crosslink by a transglutamination reaction[24]. The key to understand the mechanism of how RavJ induces actin rearrangement is to identify its target proteins. To achieve this goal, we expressed Flag-tagged RavJ or the $RavJ_{C101A}$, $RavJ_{H138A}$, $RavJ_{D170A}$ mutants in HEK293T cells. Cell lysates were subjected to immunoprecipitation with beads coated with the Flag antibody. Detection of the precipitated proteins by immunoblotting with the Flag antibody revealed that a portion of wild-type RavJ but not the mutants migrated as higher molecular weight (MW) forms (**Fig 3A**), suggesting it is posttranslationally modified. To identify the modification associated with the upshifted protein, we expressed double-tagged Flag-RavJ-His_6 in HEK293T cells and used a two-step sequential purification procedure to obtain upshifted RavJ (**Fig 3B**). Mass spectrometric analysis of proteins in the upshifted band identified abundant actin and RavJ, suggesting that the upshifted band is a product generated by protein conjugation between these two proteins.

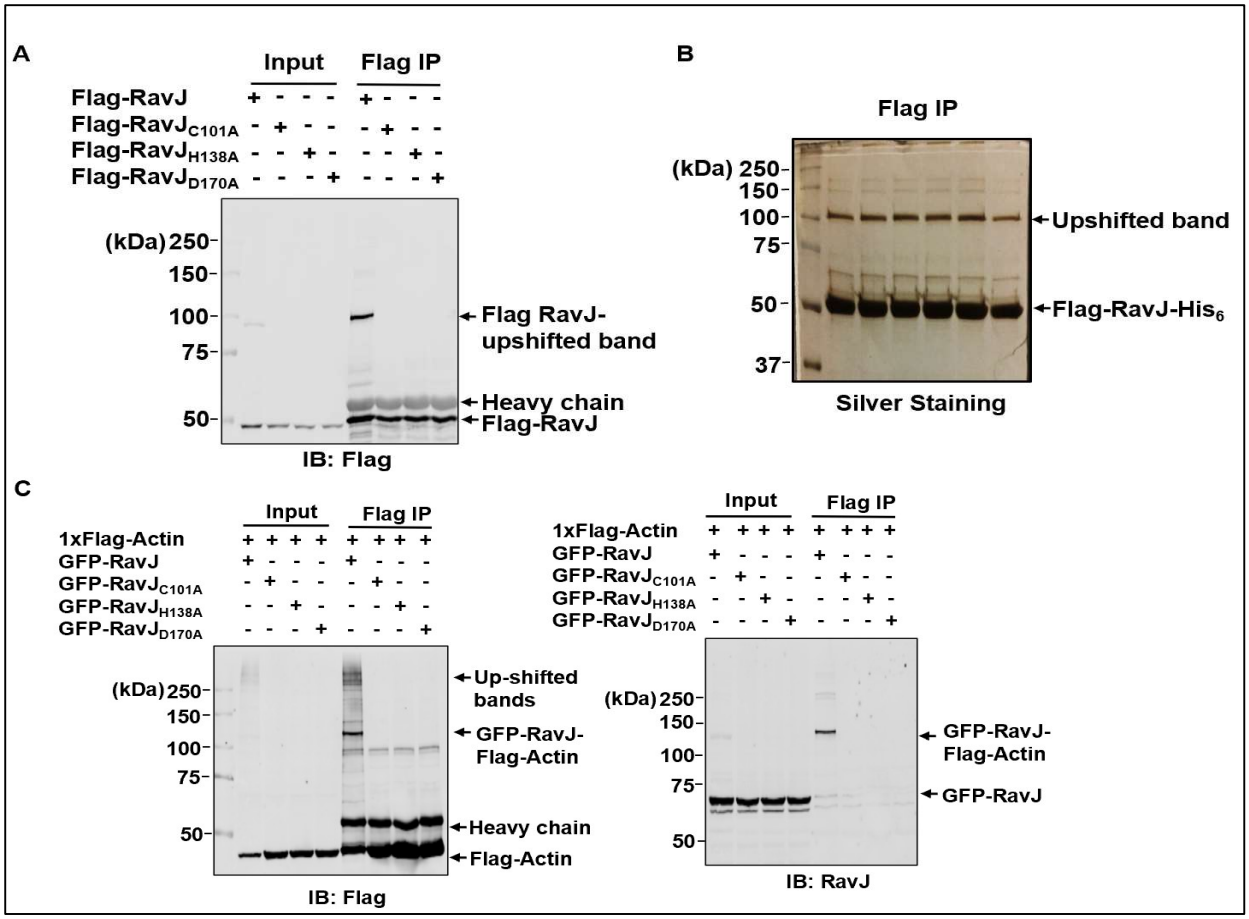

Fig 3. RavJ induces a molecular weight shift in actin by a putative transglutaminase activity. A. A portion of RavJ migrated as a higher molecular weight form when expressed in mammalian cells. HEK293T cells were transfected to express Flag-RavJ, $RavJ_{C101A}$, $RavJ_{H138A}$, or the $RavJ_{D170A}$ mutants. Total cell lysates were immunoprecipitated (IP) with beads coated with the Flag antibody. Products were resolved by SDS-PAGE and probed with the Flag antibody. Note that RavJ displayed as an upshifted band on the blot. **B**. Tandem purification of the Flag-RavJ-His_6 upshifted band. HEK293T cells were transfected to express Flag-RavJ-His_6. Cell lysates were subjected to IP with beads coated with the Flag antibody. Proteins were then eluted from the beads with 3xFLAG peptide and incubated with Ni^{2+}-NTA beads. Products were separated by SDS-PAGE and detected by silver staining. **C**. RavJ forms a covalent bond with actin in mammalian cells. HEK293T cells expressing the indicated proteins were subjected to IP with beads coated with the Flag antibody and separated by SDS-PAGE. Samples were detected by Flag-specific (left) and RavJ-specific (right) antibody, respectively.

127

128

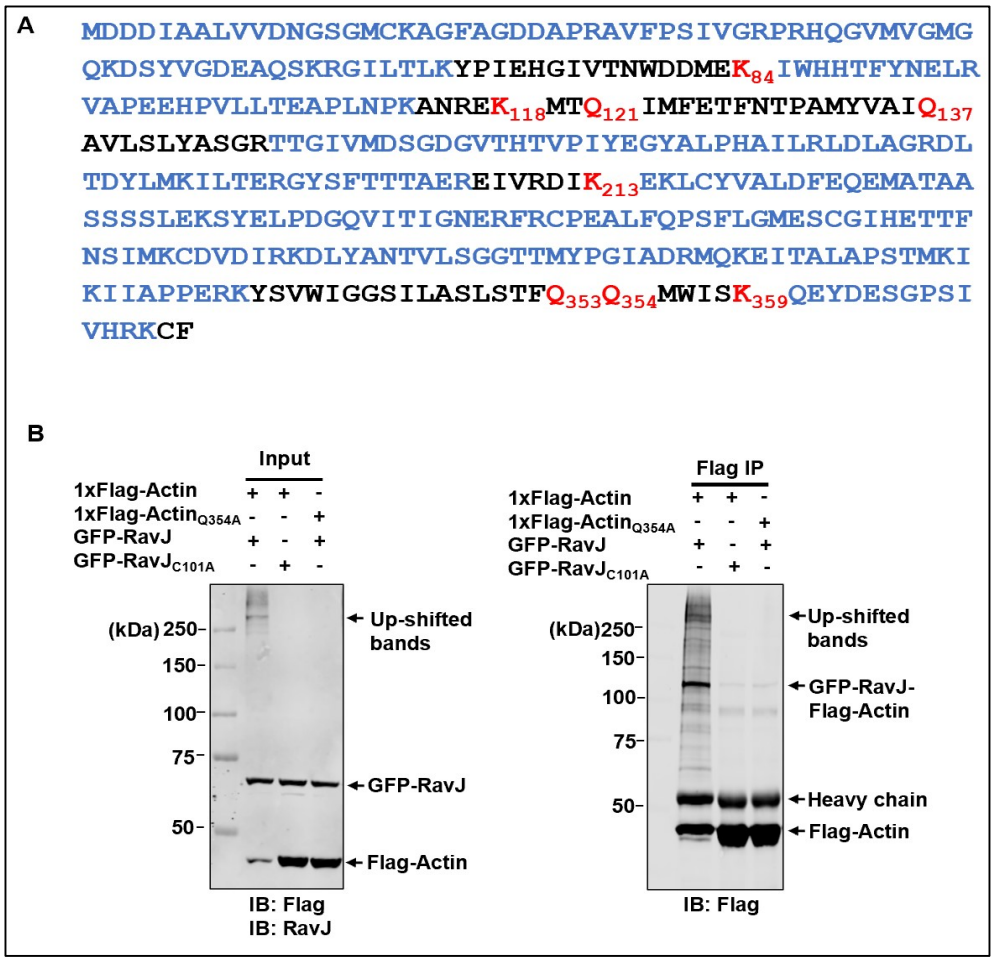

Fig 4. Actin is crosslinked to RavJ through its Gln354 residue. A. MS analysis of the Flag-RavJ-His_6 upshifted band. Coverage of the amino acids in actin are highlighted in blue. Note that Lys_{84}, Lys_{118}, Lys_{213}, Lys_{359}, Gln_{121}, Gln_{137}, Gln_{353}, Gln_{354} were not recovered from the MS, indicating them as potential linkage residues. **B.** The formation of Actin-RavJ was detected by immunoblotting. Note that the Actin Gln354Ala mutant has largely lost the ability to be modified (the 3rd lane).

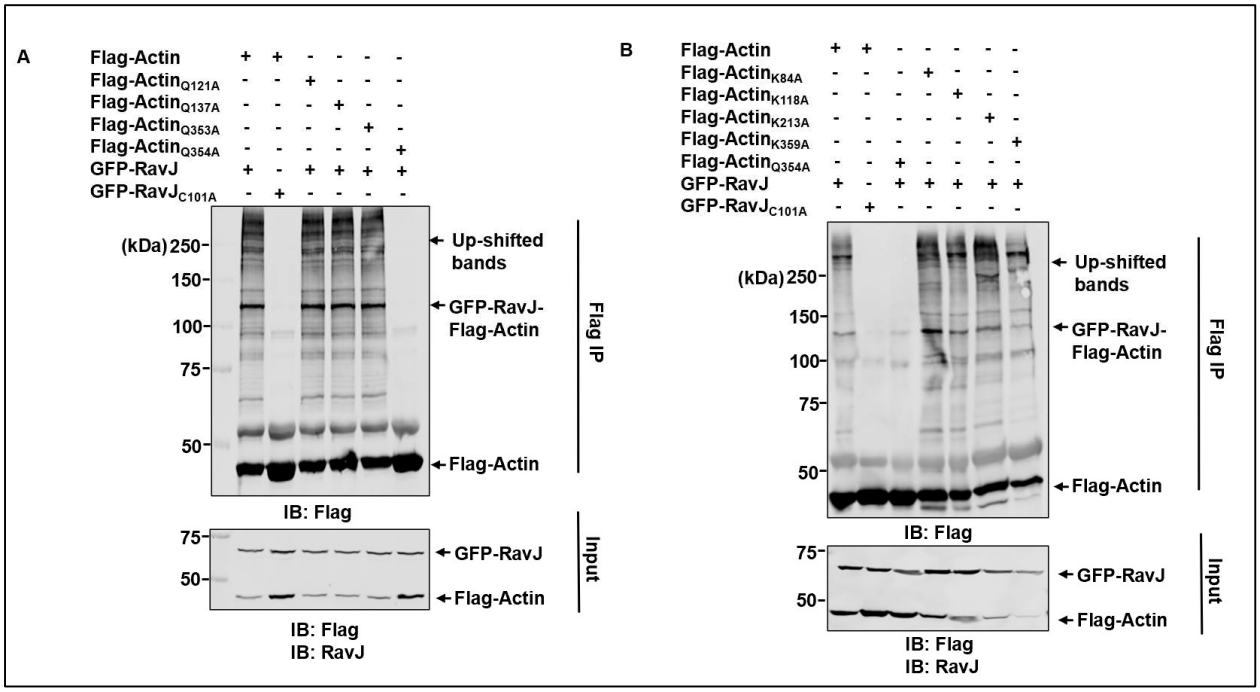

S1 Fig. Determination of the crosslink site in actin. A-B. HEK293T cells co-transfected to express the indicated proteins were lysed and immunoprecipitated by beads coated with the Flag-specific antibody. Note that only the Gln354Ala mutation in actin abolished the crosslink products induced by RavJ.

129

130 To test whether the upshifted band is a crosslink product between actin and RavJ,
131 we coexpressed Flag-tagged actin and GFP fusion of RavJ or its mutants in HEK293T
132 cells. Cell lysates were subjected to immunoprecipitation using agarose beads coated
133 with the Flag-specific antibody. We found that GFP-RavJ indeed was linked with actin
134 (**Fig 3C**). To identify the chemical linkage between actin and RavJ, the protein band
135 corresponding to the RavJ upshifted band was excised, digested with trypsin, and
136 analyzed by mass spectrometry (MS). TGs catalyze protein crosslinking by forming an
137 isopeptide bridge between the lysine (Lys) donor residue of one protein and the acceptor
138 glutamine (Gln) residue of another[24]. Thus, we hypothesized that a lysine residue and

a glutamine residue are involved in the crosslink between RavJ and actin. In the MS analysis, around 80% of the peptides in actin were recovered from the tryptic digestion, indicating Lys_{84}, Lys_{118}, Lys_{213}, Lys_{359}, Gln_{121}, Gln_{137}, Gln_{353}, Gln_{354} in actin as potential lysine donor residues or glutamine acceptor residues (**Fig 4A**). Among the individual mutation of these residues, only Q354A in actin abolished the ability of actin to crosslink with RavJ (**Figs 4B and S1A-B**).

RavJ induces crosslink between actin and members of the Motin family protein. Transglutaminases normally catalyze crosslink between two proteins, and in the absence of the receptor substrate, these enzymes induce crosslink between itself and the available donor substrate. Our analysis of the precipitated products obtained by RavJ identified a number of proteins (**Fig 3C**), one or more of which could be potentially the second substrate that crosslinks with actin in the reaction induced by RavJ. To identify such proteins, we purified the crosslink products using a tandem purification method from cells transfected to express Flag-HA-actin and GFP-RavJ. Samples similarly transfected to express the catalytically inactive $RavJ_{C101A}$ mutant were used as controls. Twenty-four hours after transfection, cell lysates were subjected to IP with beads coated with the Flag antibody. Proteins eluted with 3XFLAG peptide were further purified by IP with the HA antibody. Samples separated by SDS-PAGE were detected by immunoblotting with the appropriate antibodies. In samples transfected to express GFP-RavJ, several upshifted bands were detected with the anti-Flag antibody (**S2A Fig**). The gels containing upshifted proteins were excised, digested with trypsin, and analyzed by mass spectrometry, which allowed us to obtain a list of proteins that potentially crosslink with actin (**Table 1**). Two of Wiskott-Aldrich syndrome and SCAR homolog (WASH) complex components,

WASHC4 and WASHC5, and one protein from the Motin family, Angiomotin (AMOT) were among the proteins identified with high confidence. We considered these proteins as potential substrates of RavJ because of their relevance to the actin cytoskeleton network. Further analysis showed that RavJ did not detectably induce crosslink between actin and WASHC4 or WASHC5 (**S2B-2C Fig**). Importantly, we found that AMOT is able to form a conjugate with actin when coexpressed with RavJ (**Fig 5B**), suggesting that AMOT is the second substrate of the crosslinking reaction catalyzed by RavJ.

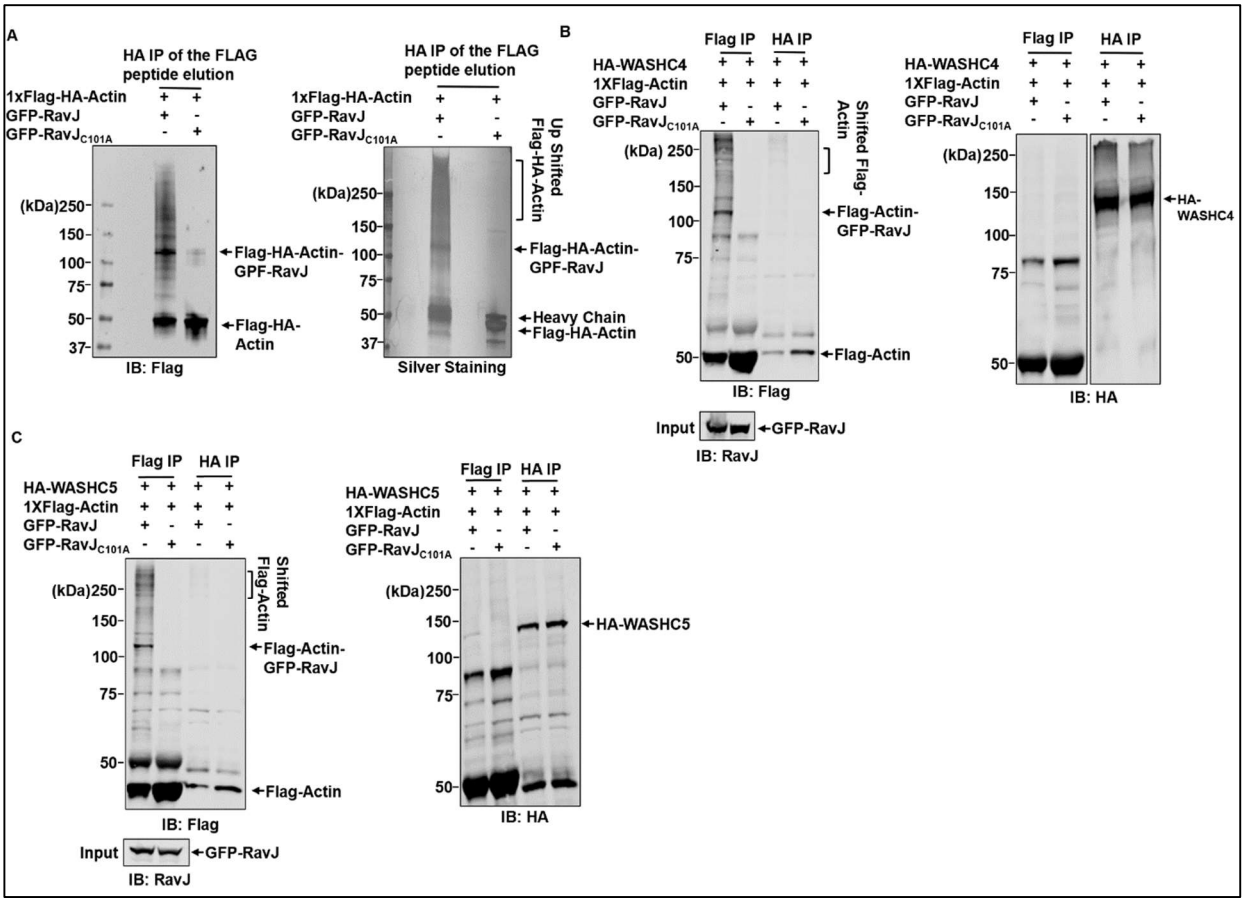

S2 Fig. Identification of the cellular targets of RavJ. A. Tandem purification of actin crosslink products catalyzed by RavJ. HEK293T cells co-transfected to express Flag-HA-Actin, GFP-RavJ or GFP-RavJ$_{C101A}$ were subjected to IP with beads coated with the Flag antibody. Proteins were eluted from the beads by 3XFLAG peptide. Elution fractions were then immunoprecipitated with beads coated with the HA-specific antibody. Products resolved by SDS-PAGE were detected by silver staining (right) or probed with the Flag antibody(left). Gel plug corresponding to the upshifted band was cut for MS analysis. **B-C**. WASHC4 and WASHC5 do not crosslink with actin in the presence of RavJ. HEK293T cells co-transfected to express the indicated proteins were lysed and immunoprecipitated by beads coated with the Flag-specific or HA-specific antibody. Note that there is no crosslink products detected between actin and WASHC4 or WASHC5.

169

Table 1: Top hits from MS analysis of the tandem purification

Protein Names	Ratio (RavJ/RavJ$_{C101A}$)	MS/MS count RavJ$_{C101A}$	MS/MS count RavJ	Mol. weight [kDa]
Actin	29.68	25	742	42
Splicing factor, proline- and glutamine-rich	19.5	2	39	76
Kinesin-like protein KIF11	17.5	6	105	119
Adenylyl cyclase-associated protein 1	7.78	14	109	51
Cytoplasmic dynein 1 heavy chain 1	∞	0	155	532
Eukaryotic translation initiation factor 4 gamma 1	∞	0	84	158
Filamin-A	∞	0	63	280
WASH complex subunit strumpellin (WASHC5)	∞	0	52	134.28
Talin-1	∞	0	44	270
Insulin receptor substrate 4	∞	0	42	133
WASH complex subunit 7 (WASHC4)	∞	0	35	136.4
Afadin	∞	0	22	210
Eukaryotic translation initiation factor 4 gamma 2	∞	0	19	98
General transcription factor II-I	∞	0	18	108
Vigilin	∞	0	17	141
Src substrate cortactin	∞	0	16	57
Angiomotin	∞	0	5	130

To verify that AMOT is targeted by RavJ, we tested the crosslink between endogenous actin and AMOT. In cells transfected to express GFP-RavJ, crosslink products formed by endogenous actin and AMOT were detected (**Fig 5C**). We also observed crosslink between actin and AMOT-p80 (**Fig 5D**), an AMOT isoform arose from alternative splicing of the *AMOT* transcript (**Fig 5A**). In addition, we have tested Angiomotin-like 1 (AMOTL1), which is another member in the Motin family having significant homology with AMOT. Crosslink products of AMOTL1 and actin were detected in HEK293T cells expressing wild-type RavJ but not its catalytically inactive mutants (**Fig 5E**). Taken together, our results indicate that RavJ catalyzes the crosslink between actin and members of the Motin family.

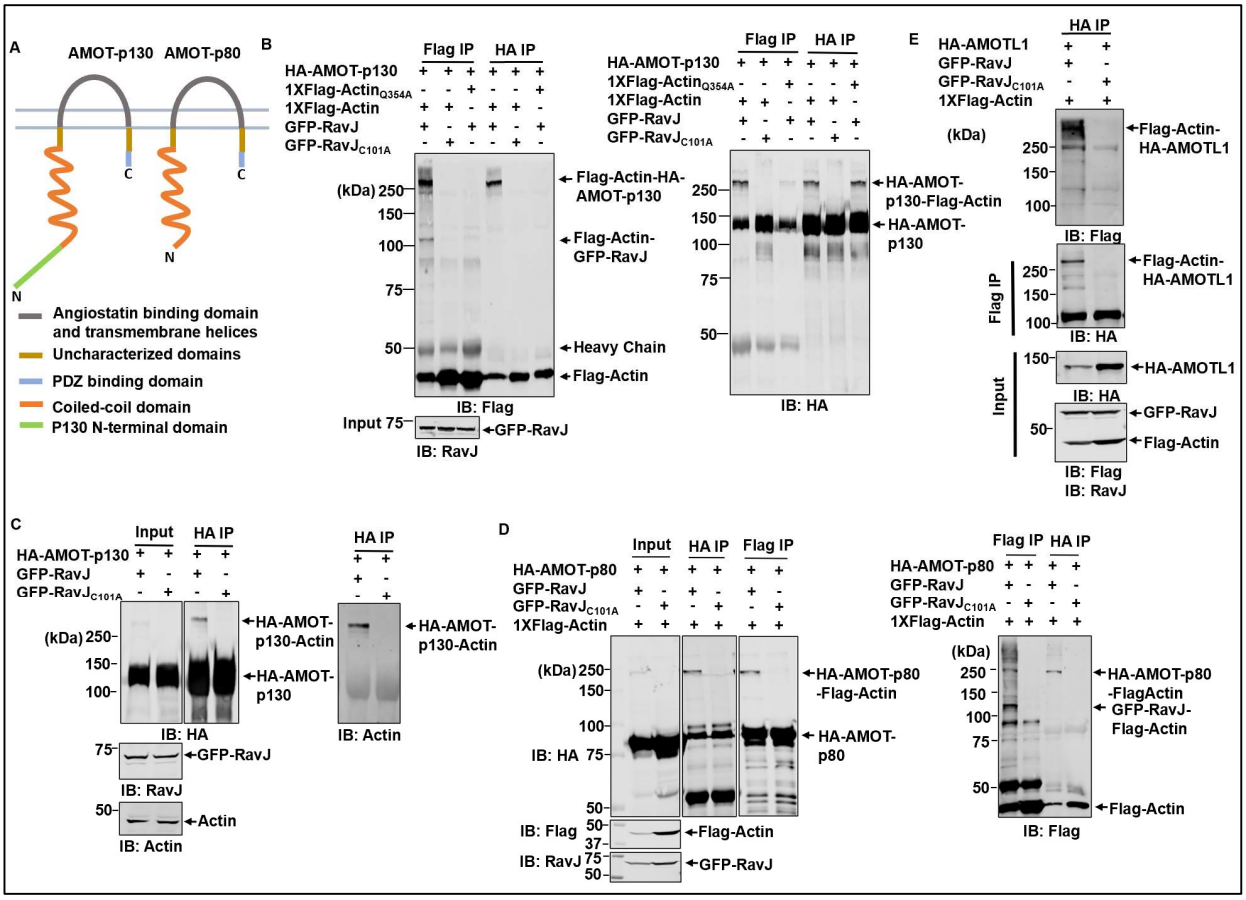

Fig 5. RavJ catalyzes crosslinks between actin and members of the Motin protein family. **A**. A schematic view of the two isoforms of AMOT produced by alternative splicing of the *AMOT* mRNA. The two isoforms, AMOT-p130 and AMOT-p80, are characterized by a conserved coiled-coil domain, a C-terminal PDZ binding domain, and an angiostatin binding domain. The AMOT-p130 isoform harbors a unique N-terminal domain. **B**. Actin conjugates with AMOT-p130 in the presence of RavJ. HEK293T cells co-transfected with the indicated proteins were lysed and subjected to IP with beads coated with the Flag antibody or the HA antibody. Samples resolved by SDS-PAGE were probed with a Flag-specific antibody or an HA-specific antibody. **C**. RavJ induces crosslink between HA-AMOT and endogenous actin. Cells expressing HA-AMOT-p130 and GFP-RavJ or the GFP-RavJ$_{C101A}$ mutant were lysed and immunoprecipitated with beads coated with the HA antibody. Crosslink products were probed by immunoblotting using either Actin or Flag antibody.

D. Actin forms a conjugate with AMOT-p80 in HEK293T cells in the presence of RavJ. Cells transfected to express the indicated proteins were lysed and subjected to IP with beads coated with Flag or HA antibody, followed by immunoblotting analysis. The proteins were detected by antibodies specific to a Flag, RavJ or HA. **E**. RavJ catalyzes the crosslink between AMOTL1 and actin. Cells transfected to express the indicated proteins were lysed and subjected to reciprocal IP, followed by SDS-PAGE analysis, and was probed with the indicated antibodies.

The Motin family of proteins harbor several structural domains, including the N-terminus domain potentially involved in Yes-associated protein 1 (YAP1) binding[28], a conserved coiled-coil (CC) domain and the C-terminal PDZ-binding domain[29] (**Fig 6A**). To determine the crosslink site on AMOT, we constructed a number of HA-tagged AMOT truncation mutants (**Fig 6A**) and tested their ability to crosslink with actin in cells expressing RavJ. Our results showed that all the four truncations were able to crosslink with actin (**Fig 6B-C and 6F**). To identify the modification sites on each truncation, the corresponding crosslink products were subjected to MS analysis (**S3A-C Fig**). However, despite multiple attempts using different enzymes to digest the crosslink products, we were unable to detect the crosslink sites between the two proteins. The mass of the peptide without the crosslink is too big to extract the peptide from the gel and to sequence it. We then mutated the two lysine residues in the truncation contains the PDZ-binding domain (**Fig 6E**). Substitution mutant in Lys_{1051} was enough to abolish the crosslink product (**Fig 6E**). The same mutation in the $AMOT_{871\text{-}1084}$ truncation also abolished the crosslink product (**Fig 6D**), suggesting that $AMOT_{871\text{-}1084}$ crosslinks with actin through its Lys_{1051} residue.

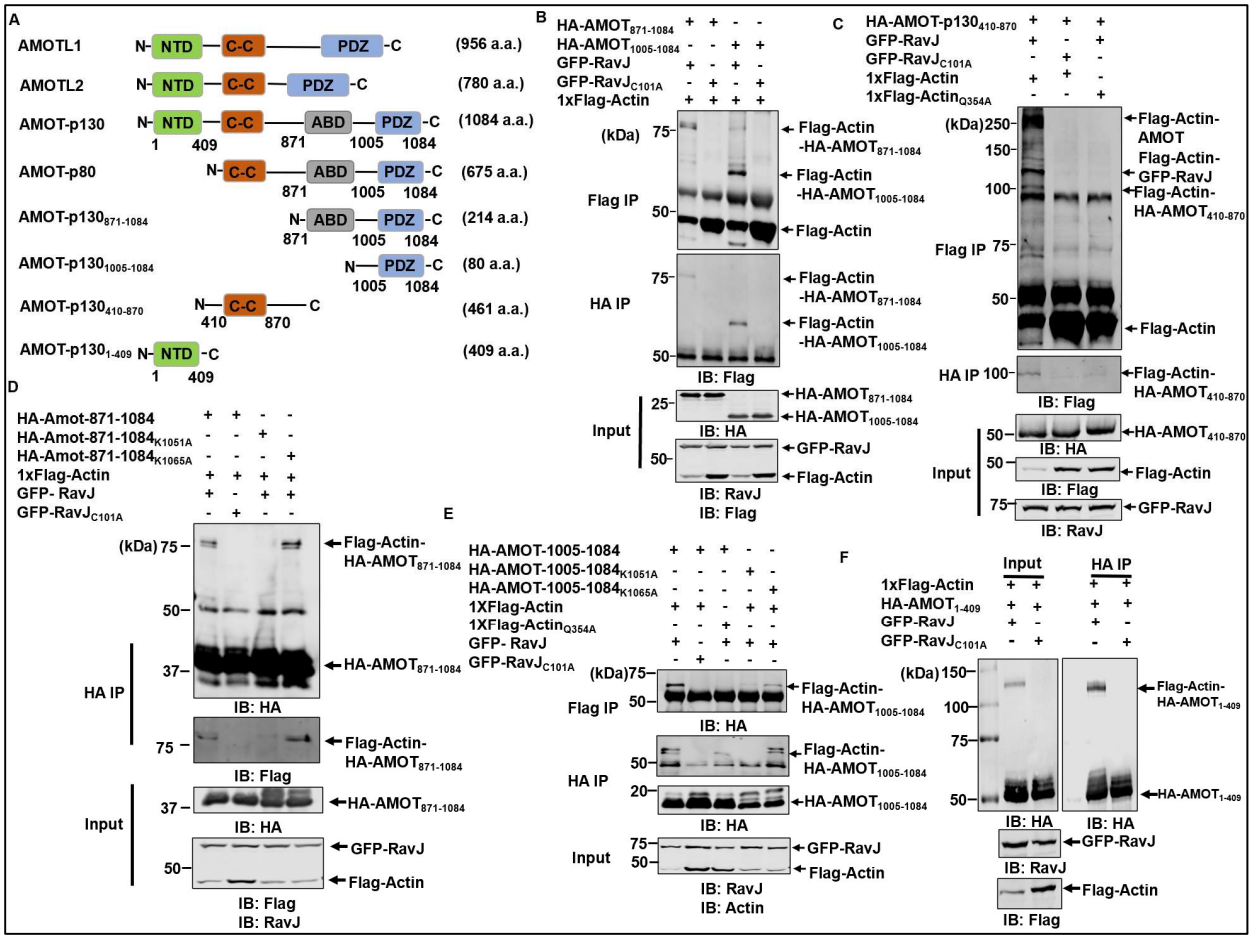

199

Fig 6. Determination of the modification sites on AMOT. HEK293T cells were transfected to express the indicated proteins. Cell lysates were subjected to reciprocal co-IP with Flag or HA antibody coated beads. Crosslink products were detected by immunoblotting with the indicated antibodies. **A**. Domain architecture of the Motin family of proteins and the AMOT-p130 truncations. The HA-tagged truncation mutants are made as indicated. **B**. The PDZ binding domain is enough to crosslink with actin. **C**. The AMOT coiled-coil truncation ($AMOT_{410-870}$) crosslinks with actin in the presence of RavJ. **D**. The $Lys_{1051}Ala$ mutation in the $AMOT_{871-1084}$ truncation abolished its ability to crosslink with actin. **E**. The $Lys_{1051}Ala$ mutation in the PDZ binding domain lost its ability to crosslink with actin. **F**. RavJ catalyzes the formation of a covalent bond between the N-terminal domain of AMOT-p130 and actin.

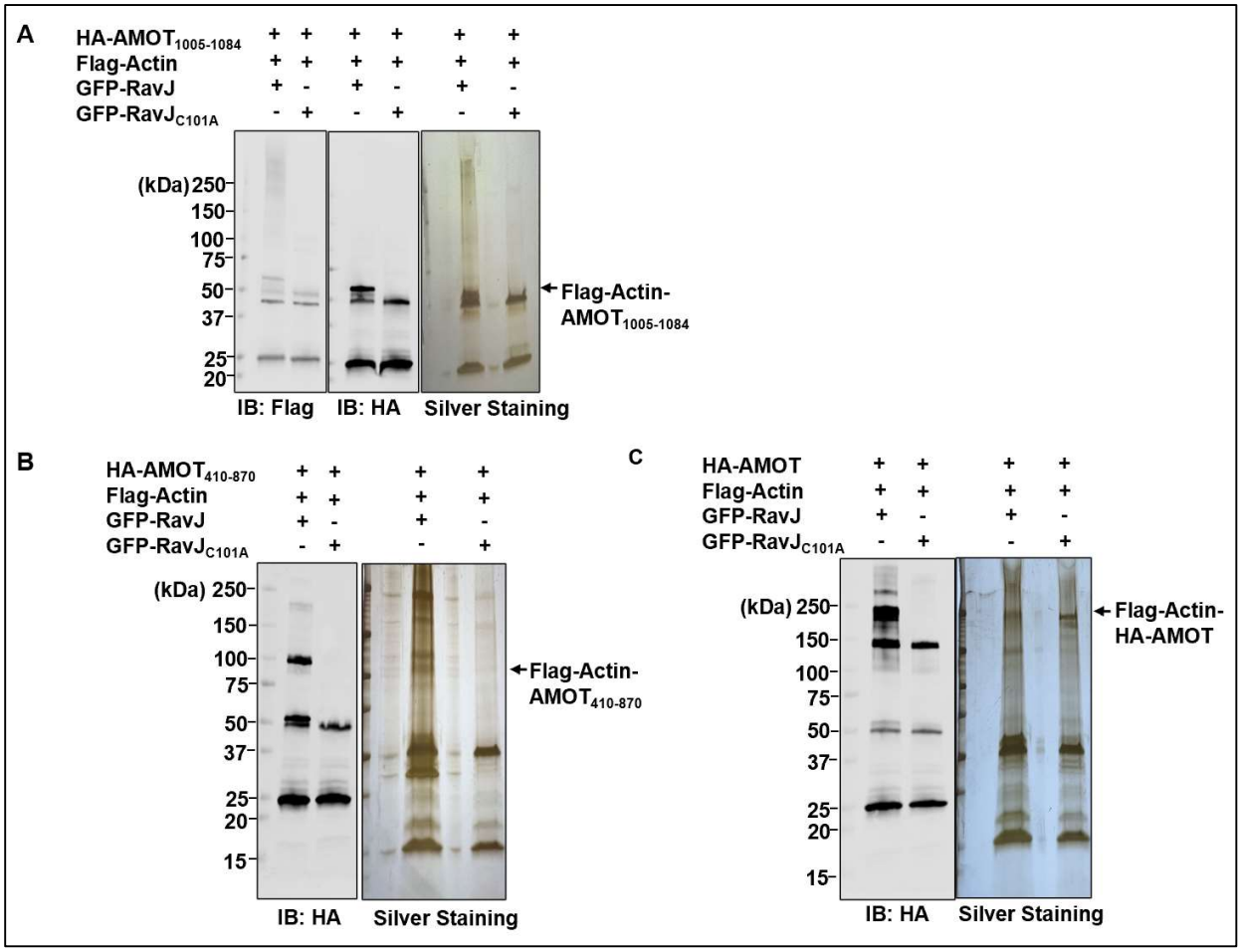

S3 Fig. Determination of the crosslink sites in AMOT. A-C. Tandem purification of crosslink products of actin and AMOT truncations. HEK293T cells co-transfected to express the indicated proteins were subjected to IP with beads coated with the Flag antibody. Proteins were eluted from the beads by 3XFLAG peptide. Elution fractions were then immunoprecipitated with beads coated with the HA-specific antibody. Products resolved by SDS-PAGE were detected by silver staining (right) or probed with the indicated antibodies(left). Protein bands corresponding to the crosslink products were excised for MS analysis.

200

201 **RavJ catalyzes crosslink between purified actin and AMOT.** We next examined
202 whether crosslink between actin and AMOT occurs in cell-free reactions. HEK293T cells

transfected to express Flag-Actin, HA-AMOT, GFP-RavJ or GFP-RavJ$_{C101A}$, respectively, were lysed, and the lysates were mixed and incubated at 37°C for 2 h. Beads coated with the Flag antibody were used to enrich Flag-Actin and products of crosslinking formed by actin and AMOT were detected by immunoblotting. Protein conjugate detectable by the HA-specific antibody was detected only in reactions that received lysates containing wild-type RavJ (**Fig 7A**), indicating that RavJ-induced crosslink between actin and AMOT occurs in a cell-free system.

To further determine the activity of this transglutaminase, recombinant RavJ purified from *E. coli* was incubated with Flag-Actin and HA-AMOT purified from HEK293T cells, and the production of a crosslink product was detected after the reactions were allowed to proceed for 2 h at 37°C (**Fig 7B**). Consistent with results from earlier experiments with cell lysates, adding His$_6$-RavJ$_{C101A}$ to the reactions did not cause crosslink between these two proteins (**Fig 7B**). Together, these results establish that RavJ is a transglutaminase that catalyzes crosslink between AMOT and actin.

***L. pneumophila* induces crosslinking between actin and AMOT in a RavJ-dependent manner.** Our results from ectopic expression by transfection strongly suggest that RavJ catalyzes protein crosslink between AMOT and actin. To determine whether this reaction is physiologically relevant, we attempted to determine the activity of RavJ during *L. pneumophila* infection. HEK293T cells transfected to express the FcγII receptor were infected with opsonized bacteria of relevant *L. pneumophila* strains at an multiplicity of infection (MOI) of 50. No crosslink between AMOT and actin was detected in cells infected with strain Lp03, an avirulent *dotA* mutant, or the wild-type stain Lp02 (**S4 Fig**). Considering the possibility that the amount of crosslinked products was too low in

samples infected with strain Lp02, we examined whether overexpression of RavJ in the wild-type strain background allows us to detect the crosslink products. Indeed, infection of the cells with strain Δ*ravJ*(pRavJ) led to robust crosslink between AMOT and actin (**Fig 7C**). In contrast, crosslink did not occur in cells similarly infected with strain Δ*ravJ*(pRavJ$_{C101A}$), which overexpressed the enzymatically inactive RavJ mutant (**Fig 7C**). These results indicate RavJ catalyzes crosslink between actin and AMOT in cells infected with *L. pneumophila* competent in the Dot/Icm system that overexpressed wild-type RavJ. The amount of crosslink products in cells infected with the wild-type strain likely was not sufficient for detection with our method, RavJ likely catalyzes the crosslink between actin and the Motin family of proteins.

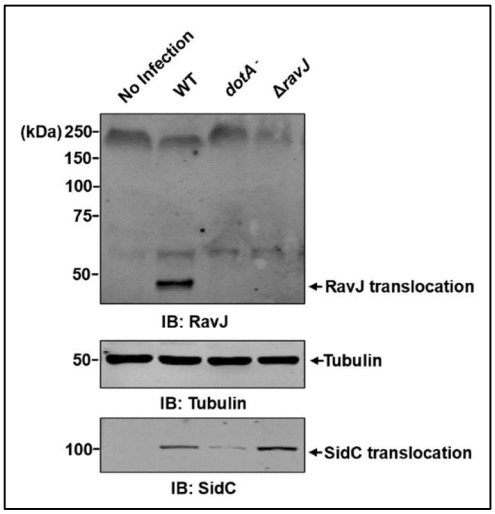

S4 Fig. Determination of the effect of RavJ during bacterial infection. HEK293T cells transfected to express the FcγII receptor were treated with opsonized bacterial strains as indicated. Cells were collected at 4 h after infection and were lysed by 0.2% saponin. RavJ and SidC translocation were detected by RavJ-specific or SidC-specific antibodies. Tubulin was probed as a loading control.

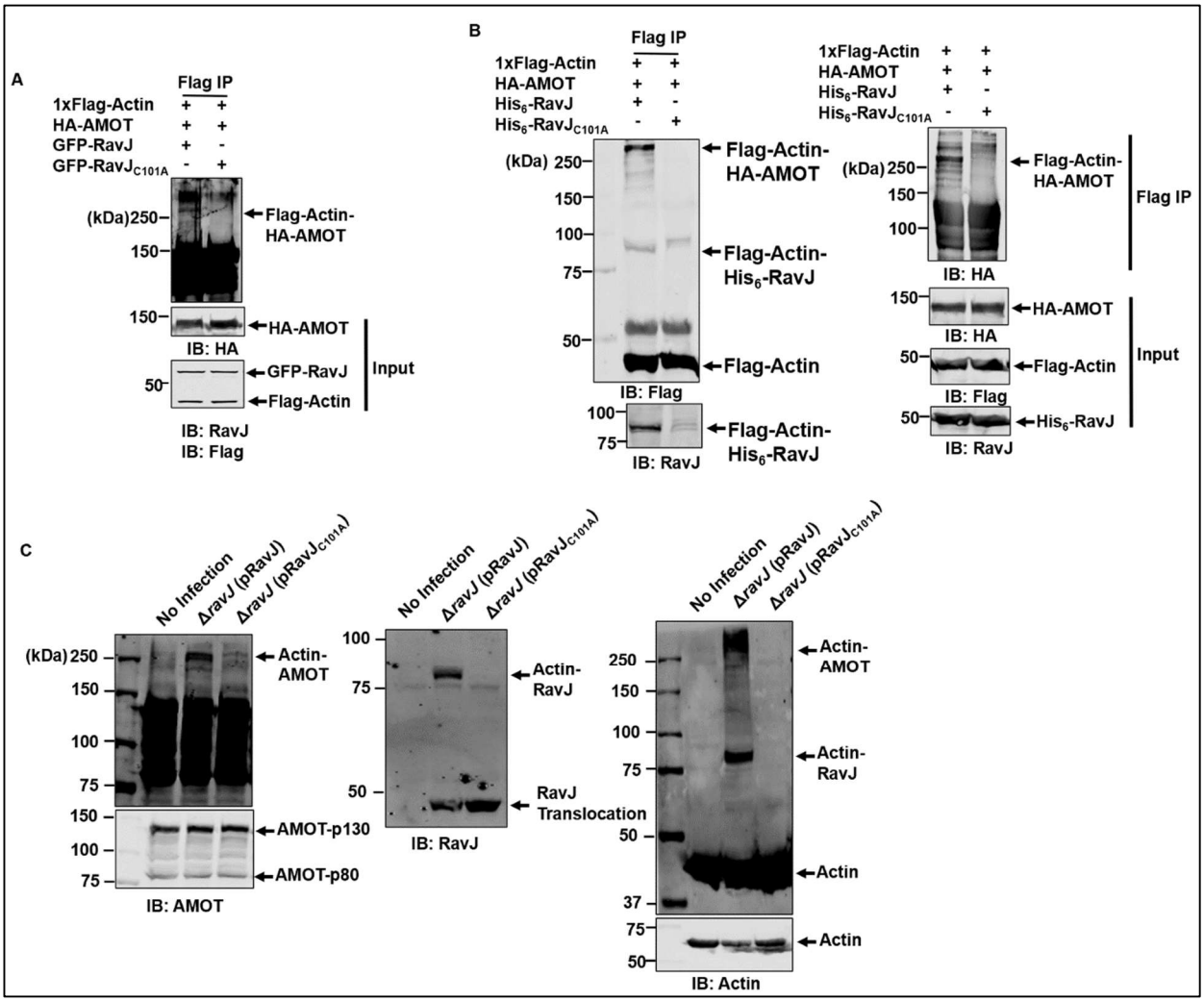

237

Fig 7. RavJ induces the formation of a protein conjugate by actin and AMOT A. RavJ catalyzes crosslink between actin and AMOT in a cell-free system. Cells transfected to express Flag-Actin, HA-AMOT, GFP-RavJ, or GFP-RavJ$_{C101A}$, respectively, were lysed with RIPA buffer without EDTA. Cell lysates were combined as indicated and incubated at 37°C for 2 h. Products were subjected to IP with beads coated with the Flag antibody, followed by immunoblotting with the indicated antibodies. **B**. RavJ induces crosslink between purified actin and AMOT *in vitro*. Reactions containing Flag-Actin, HA-AMOT, His$_6$-RavJ or His$_6$-RavJ$_{C101A}$ were incubated at 37°C for 2 h. Samples were immunoprecipitated with beads coated with the Flag antibody. The crosslink products were detected by the indicated antibodies. **C**. Crosslink between endogenous actin and AMOT was detected in cells infected with *L. pneumophila* overexpressing RavJ. HEK293T cells transfected to express the FcγII receptor were infected with the indicated bacterial strains for 4 h at an MOI of 50. Cells were lysed with 0.2% saponin and then resolved by SDS-PAGE. The blots were probed with the indicated antibodies.

238 **Simultaneous knockdown of *AMOT* and *AMOTL1* interferes with the formation of**
239 **actin filaments induced by RavJ.** Ectopic expression of RavJ in mammalian cells led to
240 the formation of actin filaments (**Fig 1**). The observation that RavJ induces protein
241 crosslink between AMOT and actin suggests that this event is important for the actin
242 polymerization phenotype. To examine the relevance between protein crosslink and the
243 formation of actin filaments, we determined the impact of AMOT depletion on RavJ-
244 induced actin filament formation. To this end, we introduced shRNAs that target mRNAs
245 of both AMOT and AMOTL1 into HEK293T cells, which is known to express high levels
246 of these two isoforms but almost an undetectable level of AMOTL2[30]. Introduction of
247 shRNAs by lentiviral transduction led to significant reduction of the protein levels of both
248 AMOT and AMOTL1 (**Fig 8A**). Next, we expressed RavJ in these cells by transfection
249 and examined the formation of actin filaments by phalloidin staining. In samples that
250 received scramble shRNAs, actin filaments were readily detected at rates similar to
251 untreated cells (**Fig 8B**). Consistently, crosslink between actin and AMOT became
252 undetectable in these cells (**Fig 8C**). Furthermore, overexpression of AMOT by
253 transfection rescued not only RavJ-induced formation of actin filaments but also the
254 crosslink between actin and AMOT (**Fig 8B-C**). Taken together, these results support a
255 conclusion that members of the Motin family of proteins are important for RavJ-induced
256 actin accumulation by forming protein conjugates with actin.

257

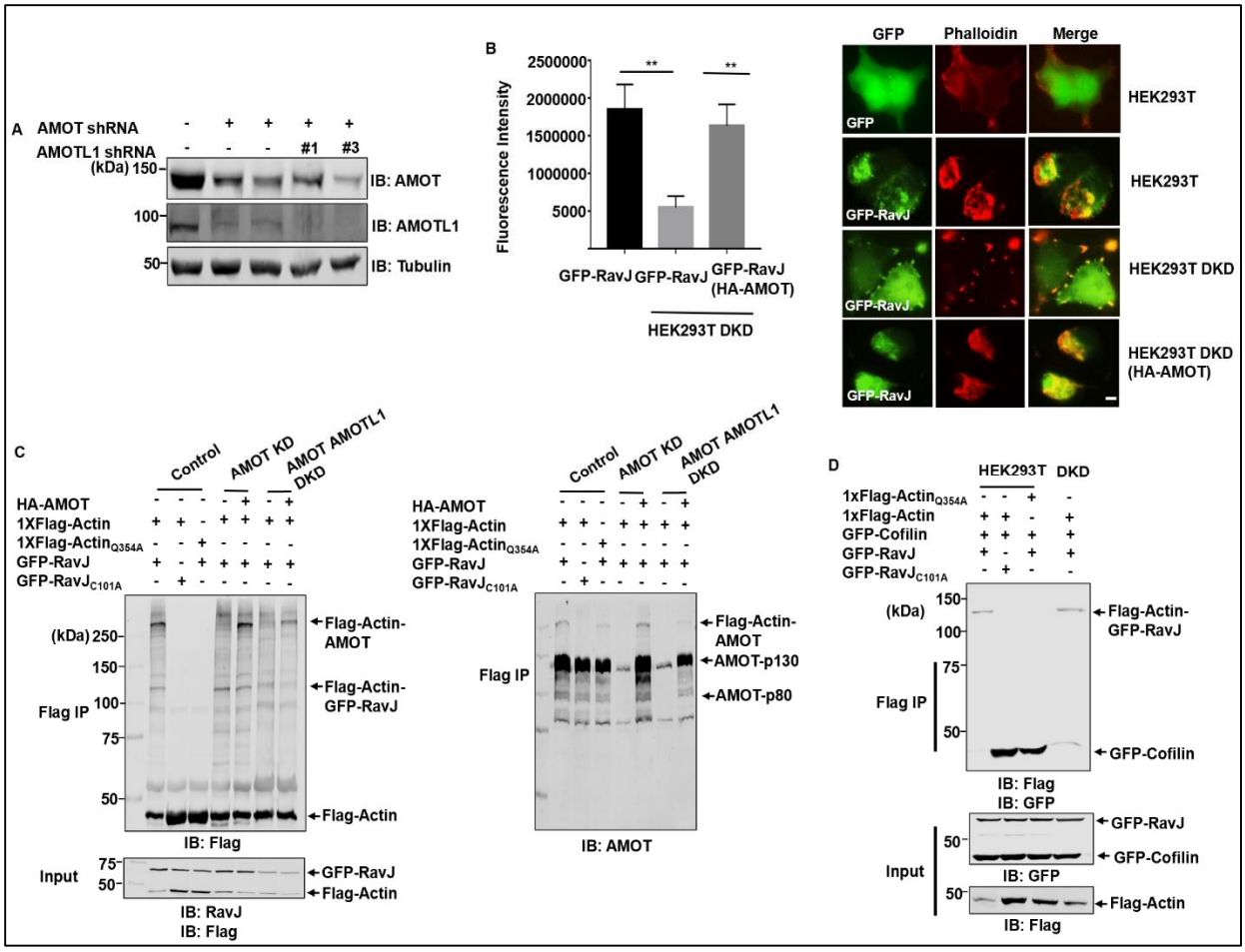

Fig 8. Knockdown of AMOT and AMOTL1 reduced actin accumulation in HEK293T cells induced by RavJ. **A**. Expression level of AMOT and AMOTL1 was examined by Western blot. The expression of the proteins was probed in cell lysates of two clones of AMOT knockdown cells and two clones of AMOT and AMOTL1 double knockdown cells. Proteins were detected by an AMOT-p130-specific antibody and an AMOTL1-specific antibody. Tubulin was detected as a loading control. **B**. AMOT and AMOTL1 double knockdown in HEK293T cells significantly reduced actin accumulation in cells expressing wild-type RavJ. Cells transfected to express the indicated proteins were fixed and stained with phalloidin conjugated with Texas-red. Bar, 10 μm. Phalloidin fluorescence signal was quantified by Image J software to evaluate the amount of F-actin (the left panel). Data are the mean SEM (***p<0.001). **C**. Knockdown of AMOT and AMOTL1 in HEK293T cells abolished crosslink between actin and the Motin family of protein. Cells were transfected to express the indicated proteins and samples were subjected to IP with beads coated with the Flag antibody. Crosslinking products were detected with the Flag-specific antibody and AMOT-specific antibodies, respectively.

D. RavJ inhibits the binding between actin and cofilin. Cells transfected to express the indicated proteins were lysed and subjected to IP with beads coated with the Flag-specific antibody. Binding between actin and cofilin were detected by the indicated antibodies.

RavJ interferes with the interaction between actin and cofilin. Earlier studies suggest that actin interacts with profilin and cofilin through its Gln_{354} residue[31-33]. Cofilin depolymerizes and severs actin filaments while profilin binds to actin monomers and provides ATP-Actin for incorporation into actin filaments[34]. The fact that actin crosslinks with RavJ and AMOT via Gln_{354} inspired us to investigate whether RavJ affects the binding between actin and actin binding proteins. HA-profilin-1, HA-profilin-2 or GFP-cofilin were expressed in HEK293T cells along with relevant proteins, and cell lysates were subjected to immunoprecipitation with the Flag-specific antibody. Interestingly, expression of RavJ reduced the binding between actin and cofilin (**Figure 8D**), but not profilin-1 and profilin-2 (**S5A-B Fig**), suggesting that RavJ-induced actin accumulation in cell cortex was a result of reduced actin depolymerization.

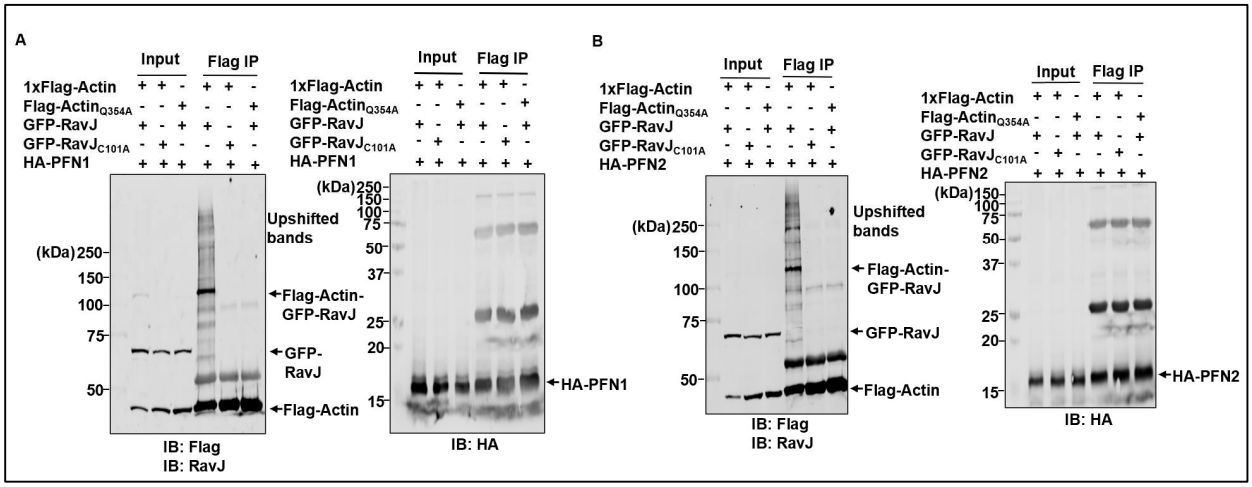

S5 Fig. Effects of RavJ on the binding between actin and actin binding proteins. A-B. RavJ does not influence the binding between actin and actin binding proteins, profilin 1 and profilin 2. HEK293T cells co-transfected to express the indicated proteins were lysed and subjected to IP with beads coated with a Flag-specific antibody.

LegL1 blocks the activity of RavJ by sterically hindering its catalytic site. In a previous study, LegL1 (Lpg0945) was identified as a putative metaeffector of RavJ which interacts with its amino terminus containing the predicted motif important for its enzymatic activity[27]. We then tested whether LegL1 can influence actin cytoskeleton rearrangement induced by RavJ. Coexpression of HA-LegL1 with GFP-RavJ significantly reduced the formation of crosslink products by actin and AMOTs and such reduction became more apparent as the ratio between LegL1 and RavJ increased (**Fig 9A**), indicating that LegL1 inhibits the activity of RavJ. The inhibitory effect of LegL1 can attribute to at least two potential mechanisms: LegL1 reverses the crosslink by an enzymatic activity, or it inhibits the activity of RavJ by direct binding.

To distinguish between these two possibilities, we pre-incubated cell lysates expressing HA-LegL1 with cell lysates expressing GFP-RavJ for 1 h at 37°C. Cell lysates expressing HA-AMOT and Flag-Actin, respectively, were then added to the cell-free system. RavJ that has been pre-incubated with HA-LegL1 was unable to induce crosslink between actin and AMOT, suggesting that LegL1 blocks the activity of RavJ (**Fig 9B**). Furthermore, addition of HA-LegL1 to reactions containing crosslinked actin-AMOT did not detectably reduce the amount of the conjugate product (**S6 Fig**). We also tested the activity of recombinant LegL1 purified from *E. coli.* Incubation of GST-LegL1 with cell lysates expressing GFP-RavJ ablated its ability to catalyze crosslink between actin and AMOT (**Fig 9D**).

We next examined the interactions between LegL1 and RavJ in *L. pneumophila*. RavJ can be immunoprecipitated from lysates of *L. pneumophila* expressing Flag-LegL1 with beads coated with the Flag antibody, indicating binding between LegL1 and RavJ (**Fig 9E**). We further tested the effect of LegL1 on RavJ-induced crosslink during bacterial infection. HEK293T cells were infected with *ravJ* mutant complemented with RavJ, the $RavJ_{C101A}$ mutant, or both RavJ and LegL1, at an MOI of 50. Crosslink between AMOT and actin was only detected in cells infected with the Δ*ravJ*(pRavJ) strain but not strain Δ*ravJ*(pRavJ, pLegL1) (**Fig 9C**), suggesting that LegL1 effectively inhibits the crosslink caused by RavJ during bacterial infection. The translocation of RavJ into host cells is not influenced by LegL1, indicating that the regulation of RavJ by LegL1 is likely occurs in the host cells (**Fig 9F**). Collectively, these results indicate that LegL1 blocks the activity of RavJ by direct binding.

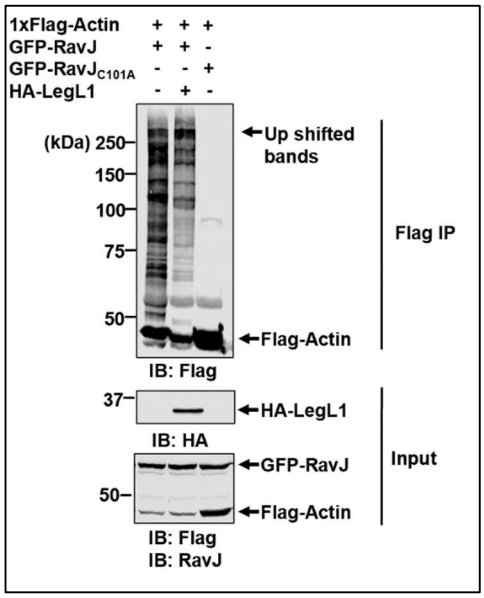

S6 Fig. LegL1 does not reverse the transglutaminase activity of RavJ. HEK293T cells transfected to express the indicated proteins were lysed and subjected to IP with beads coated with the Flag-specific antibody. Note that expression of HA-LegL1 did not remove actin from the crosslink product.

304

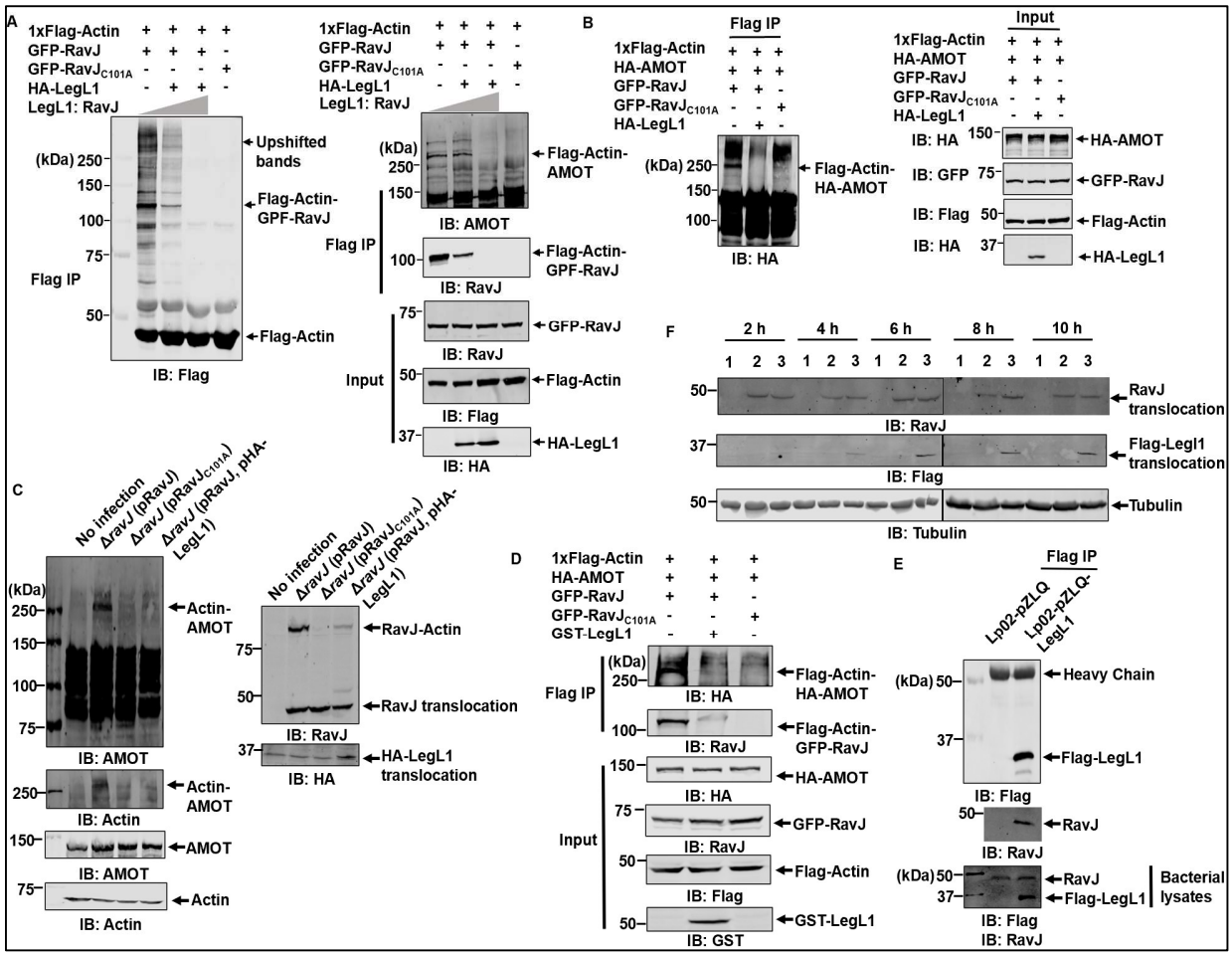

Fig 9. LegL1 antagonizes the catalytic activity of RavJ. A. expression of LegL1 in HEK293T cells reduced crosslink products induced by RavJ. Lysates of cells transfected to express the indicated proteins were subjected to IP with beads coated with the Flag antibody and the products resolved by SDS-PAGE were detected with the indicated antibodies. **B**. LegL1 inhibits the activity of RavJ in a cell-free system. Cells transfected to express Flag-Actin, HA-LegL1, HA-AMOT, GFP-RavJ, and GFP-RavJ$_{C101A}$, respectively, were lysed with RIPA buffer without EDTA. Lysates of HA-LegL1 was pre-incubated with those expressing GFP-RavJ for 1 h at 37°C. Reactions containing the indicated cell lysates were immunoprecipitated with beads coated with the Flag antibody and proteins were detected with the indicated antibodies. **C**. Overexpression of LegL1 in *L. pneumophila* inhibits the enzymatic activity of RavJ. Bacteria of the indicated *L. pneumophila* strains were opsonized prior to infecting HEK293T cells transfected to express the FcγII receptor at an MOI of 50 for 4 h. Cells lysed with 0.2% saponin were probed with the indicated antibodies.

D. Recombinant LegL1 reduces the crosslink products induced by RavJ. Cells transfected to express Flag-Actin, HA-AMOT, GFP-RavJ, and GFP-RavJ$_{C101A}$, respectively, were lysed with RIPA buffer without EDTA. 10 μg GST-LegL1 was pre-incubated with cell lysates of GFP-RavJ for 1 h at 37°C. Reactions containing the indicated components were immunoprecipitated with beads coated with the Flag antibody and proteins were detected with the indicated antibodies. **E**. LegL1 directly binds to RavJ in *L. pneumophila.* Bacterial cells carrying either the vector pZLQ or pZLQ-LegL1 were lysed with RIPA buffer and then immunoprecipitated with beads coated with the Flag antibody. Binding between RavJ and LegL1 was detected by RavJ-specific antibodies and the Flag antibody, respectively **F**. Overexpression of LegL1 in *L. pneumophila* does not influence the translocation of RavJ. HEK293T cells transfected to express the FcγII receptor were treated with different bacterial strains: 1. No infection, 2. Wild-type *L. pneumophila*. 3. Wild type *L. pneumophila* overexpressing Flag-LegL1. Cells were collected at the indicated time points and lysed by 0.2% saponin. RavJ and LegL1 translocation were detected by RavJ-specific antibodies and the Flag-specific antibody respectively. Tubulin was probed as a loading control.

305

Discussion

The actin cytoskeleton network is a major host structural component that provides structural and functional support in numerous vital cellular activities. It also directs the trafficking of cargo-containing vesicle trafficking throughout the cell by functioning as a highway[35]. Intracellular bacterial pathogens have evolved remarkable strategies to subvert the host cytoskeletal machinery to promote bacterial internalization, facilitate the biogenesis of bacteria-containing phagosomes, and co-opt actin-dependent movement to benefit pathogen dissemination[36]. To support diverse infection events, intracellular pathogens hijack the actin cytoskeleton by introducing effector proteins into the host cytosol by specialized secretion systems[8]. Among these, *Coxiella burnetii* triggers actin reorganization at the attachment site of phagocytic human macrophages by binding to CR3 receptors to stimulate bacterial internalization[37]. After entering a host cell, this bacterium replicates within an acidic compartment called the parasitophorous vacuole (PV) in macrophages. Optimal intracellular growth of *C. burnetii* requires F-actin accumulation around the PV, but the detailed mechanisms are not fully characterized[38]. *Chlamydia* species replicate in a host membrane-derived compartment termed inclusion. Optimal development and maintenance of vacuole morphology and integrity require F-actin rings surrounding the inclusion to stabilize the organelle[39, 40]. Spotted Fever Group *Rickettsia*, such as *R. rickettsii* and *R. conorii*, escape the phagosome before lysosomal fusion after entering a host cell. After escape, these bacteria induce actin polymerization to form an actin tail that facilitates bacterial motility within the cell[41, 42].

Actin exists in two main forms of organization, the monomeric G-actin, and the filamentous form F-actin[43]. Polymerization and depolymerization of actin filaments are

kept in a dynamic balance to tightly regulate movement and other cell functions[43]. The VCA domains of N-WASP (Wiskott-Aldrich syndrome protein) and SCAR/WAVE (suppressor of Camp receptor/WASP-family verprolin homologous protein) activate the actin nucleator Arp2/3 complex to generate new F-actin branches from preexisting mother filaments[44]. Actin-depolymerizing factor ADF/cofilin regulates actin dynamics by depolymerizing filaments at their pointed ends, thereby restoring a pool of actin monomers for filament assembly[35]. Actin molecule harbors two main lobes separated by a deep upper cleft. Each main lobe is subdivided into two clearly discernible subdomains, SD1-4[45]. SD1, which is built from residues 1-32, 70-144, and 338-375, forms an important target area for a large number of actin-binding proteins such as profilin, cofilin and gelsolin[45]. Of note is that RavJ-induced actin crosslink with AMOT occurs at Gln354, a site locates on the SD1, suggesting that this crosslinking event may interfere with the interaction between actin subunits in the filament and the actin binding proteins. In agreement with this notion, the binding between cofilin and actin is significantly reduced (**Fig 8D**), indicating that RavJ functions to block actin depolymerization, resulting in the accumulation of F-actin in cell cortex.

It has been known for a long time that *L. pneumophila* avoids the delivery of its vacuole to lysosomes by modulating the ER-to-Golgi vesicle trafficking[46]. Shortly after being internalized by a host cell, the plasma membrane derived vacuole containing *L. pneumophila* will be converted into a compartment that has similarity to an ER-Golgi intermediate compartment[47-49]. The biogenesis of this specialized phagosome has been studied extensively[49]. A repertoire of Dot/Icm effectors have been demonstrated to hijack the host vesicle trafficking pathway directly[2, 50], some of them could affect this

cellular process indirectly to bypass the microbicidal endosomal compartment[51]. The modulation of the actin cytoskeleton clearly contributes to the development of the LCV. For example, the metal protease RavK cleaves actin, abolishing its ability to form actin polymers[11] whereas LegK2 phosphorylates components of actin nucleator ARP2/3 complex and thus inhibits actin polymerization on the phagosome[11]. Ceg14 inhibits actin polymerization by a yet unknown mechanism[13]. These proteins are very likely working in synergic to temporally inhibit actin polymerization on the LCV and thus preventing fusion with late endosomes[12]. In contrast to the inhibitory effects of RavK and LegK2, VipA enhances actin polymerization by acting as an actin nucleator[14]. RavJ also appears to promote the formation of actin filaments. Here, we showed that RavJ-induced crosslink between actin and AMOT blocks the depolymerization activity of ADF/cofilin, resulting in the stabilization of actin polymers in cell cortex (**S7 Fig**). Clearly, in cells infected with *L. pneumophila*, its effectors strike a balance between the two states of actin. Balanced modulation of host processes has recently emerged as a prominent feature associated with the interactions between *L. pneumophila* and its hosts. In some cases, the balance is achieved by effector pairs with opposite biochemical activity which may function at different phases of infection[52]. In other cases, the importance of balance lies in the cellular locations of the molecular events regulated by the effectors[17]. In addition to other effectors that inhibit actin polymerization, the regulation imposed by RavJ is controlled by its metaeffector LegL1, which blocks its function by direct protein-protein interactions. LegL1 likely functions to spatially and temporally prevent RavJ from inducing excessive actin polymerization.

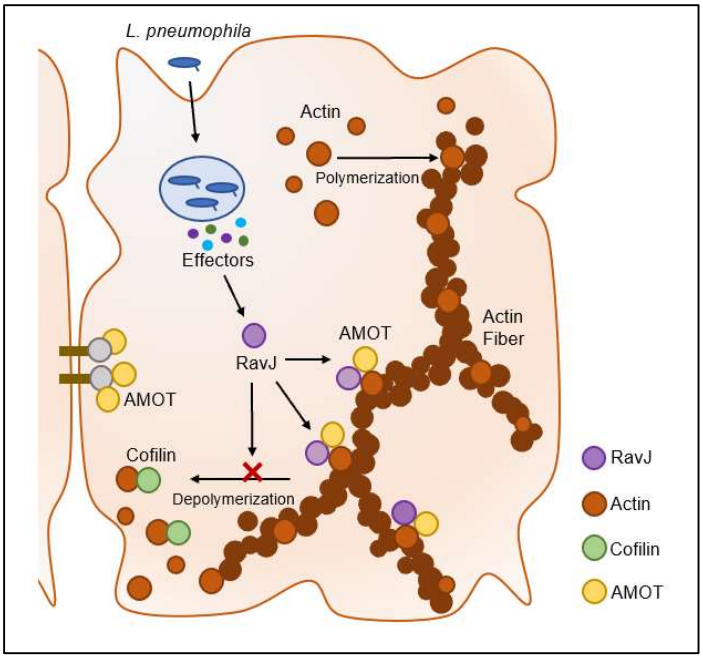

374

S7 Fig. A predicted model of RavJ in actin cytoskeleton modulation. RavJ catalyzes the crosslink between actin and AMOT, which led to the blockage of the ADF/cofilin binding site in actin, resulting in stabilization of actin fibers in the cell cortex.

375

376 Clathrin-vesicle associated proteins regulate vesicle assembly by binding directly
377 to the actin filaments through a C-terminal talin-like domain, indicating important
378 correlation between actin polymerization and endocytic vesicle trafficking[53]. Actin
379 filaments also play a key role in maintaining ER structure and the ER-to-Golgi
380 trafficking[54]. Given the extensive interconnection between vesicle trafficking and the
381 actin cytoskeleton, RavJ is likely working in concert with VipA to enhance cargo
382 transportation between ER and the LCV, thus facilitating fusions between the ER-derived
383 vesicles and the LCV. Together, these effectors are likely work in concert to promote
384 bacterial replication by indirectly interfering with the vesicle trafficking pathway.

Materials and Methods

Media, bacteria strains, and cell lines. *E. coli* strain DH5a was used for cloning and plasmid construction strains XL1-Blue and BL21(DE3) were used for expression and purification of all the recombinant proteins used in this study. *E. coli* strains were grown on LB agar plates or in LB broth. When necessary, antibiotics were added to media at the following concentrations: ampicillin, 100 μg/ml; kanamycin, 30 μg/ml. *L. pneumophila* strains used in this study were derivatives of the Philadelphia 1 strain Lp02[55]. Lp03 is an isogenic *dotA*$^{-}$ mutant of Lp02[56]. All strains were grown and maintained on CYE plates or in ACES-buffered yeast extract (AYE) broth as previously described[55]. For *L. pneumophila*, kanamycin was used at 30 μg/ml. When needed, thymidine was added at a final concentration of 100 μg/ml for thy autotrophic strains. The *ravJ* in-frame deletion strain was constructed by a two-step allelic exchange strategy as described previously[57]. HEK293T cells purchased from ATCC were cultured in Dulbecco's modified minimal Eagle's medium (DMEM) supplemented with 10% fetal bovine serum (FBS). Bone marrow-derived macrophages (BMDMs) were isolated and cultured as described previously[58]. All cell lines were regularly checked for potential mycoplasma contamination by the universal mycoplasma detection kit from ATCC (cat# 30-1012K).

Plasmid constructions. All the plasmids used in this study are listed in Table S1 and the bacterial strains and antibodies are in Table S2. For protein purifications, *ravJ*, *ravJ*$_{C101A}$, and *legI1* were cloned into pQE30 (QIAGEN) or pGEX6p-1, respectively. For complementation experiments, *ravJ* and *ravJ*$_{C101A}$ were inserted into pZLQ-Flag, a derivative of pZLQ[59] that was modified to carry a Flag tag[60]. *legI1* was inserted into either pZLQ-Flag or pZL507[61] for overexpression in *L. pneumophila.* For ectopic

expression of proteins in mammalian cells, genes were inserted into the 4xFlag CMV [20], pFlag-CMV (Sigma), pEGFP-C1 (Clontech) vector, 3XHA pCDNA3.1 vector[62] or pAPH[63], a derivative of pVR1012 suitable for expressing proteins with an amino terminal HA tag. Human *AMOT* and *AMOTL1* were amplified from cDNAs of HEK293T cells and then inserted into BamHI/SalI of pAPH. For shRNA knockdown of *AMOTL1* in mammalian cells, pLKO.1-hygro vector (Addgene, plasmid #24150) was used to generate the pLKO.1-hygro-*AMOTL1*-sh construct. Packing plasmids psPAX2(Addgene, plasmid #12260) and pMD2.G (Addgene, plasmid #12259) were used for lentiviral constructs transduction.

Transfection, immunoprecipitation, infection. HEK293T cells grown to about 90% confluence were transfected with different plasmids, respectively, using Lipofectamine 3000 (Thermo Fisher Scientific). Transfected cells were collected and lysed with radioimmunoprecipitation assay buffer (RIPA buffer, Thermo Fisher Scientific) at 18-24 h post transfection. When needed, immunoprecipitation was performed with lysates of transfected cells with Flag- or HA-specific antibody-coated agarose beads (Sigma-Aldrich, cat# F2426, Pierce, cat# 88836, respectively) at 4°C overnight. Beads were then washed with pre-cold RIPA buffer three times. For tandem purification, followed by RIPA wash, agarose beads with flag-tagged proteins were washed with Flag-to-His buffer (100 mM Na-Phosphate, pH 8.0, 150 mM NaCl, 0.05% Triton X-100) three times and eluted with 3XFLAG peptide (Sigma-Aldrich, cat# F3290). Elution fraction was then subjected to HA beads, or Ni^{2+}-NTA agarose beads (QIAGEN) as needed. Beads were resolved by SDS-PAGE gels followed by immunoblotting analysis with specific antibodies or silver staining following the manufacturer's protocols (Sigma-Aldrich, cat# PROTSIL1).

For infection experiments, *L. pneumophila* strains were grown to post-exponential phase (OD_{600}=3.2-3.8) in AYE broth. Complementation strains and overexpression strains were induced with 0.5 mM IPTG for 2 h at 37°C before infection. HEK293T cells were transfected to express FcγII receptor[20]. *L. pneumophila* strains were incubated with *L. pneumophila*-specific anti-sera at a dilution of 1:500 for 30 minutes at 37°C. Cells were infected at an MOI of 50 for 4 h and then lysed with 0.2% saponin. Cell lysates were resolved by SDS-PAGE and followed by immunoblotting analysis with the specific antibodies.

Antibodies and immunoblotting. Purified His_6-RavJ was used to raise rabbit specific antibodies following a standard protocol (Pocono Rabbit Farm & Laboratory). The antibodies were affinity-purified as described before[64]. For immunoblotting, samples resolved by SDS-PAGE were transferred onto 0.2 μm nitrocellulose membranes (Bio-Rad, cat# 1620112). Membranes were blocked with 5% non-fat milk, incubated with the appropriate primary antibodies: anti-HA (Sigma-Aldrich, cat# H3663), 1:5000; anti-tubulin (DSHB, E7), 1:10000, anti-Flag (Sigma-Aldrich, cat# F1804), 1:5000, anti-RavJ (this study), 1:5000, anti-Actin (MP Biomedicals, cat# 0869100), 1:5000, anti-AMOTL1 (Sigma-Aldrich, cat# SAB1408393), 1:5000, anti-AMOT (Abnova, cat# H00154796-B01P), 1:5000, anti-ICDH[61], 1:10000, anti-GFP[61], 1:10000, anti-GST[61]. Membranes were then incubated with an appropriate IRDye infrared secondary antibody and scanned by an Odyssey infrared imaging system (Li-Cor's Biosciences).

Immunostaining. HEK293T cells were seeded at $1X10^5$ per well on glass coverslips in 24-well plates. Cells were transfected to express the corresponding proteins for 24 h and were washed three times with PBS. Cells were fixed with 4% formaldehyde for 30 minutes

454 at room temperature, washed with PBS three times and were then permeabilized by 0.3%
455 Triton at room temperature for 15 minutes. F-actin was stained with phalloidin conjugated
456 with Texas-red (Thermo Fisher Scientific, cat#T7471) at a dilution of 1:500 for 1 h at room
457 temperature. Images were acquired using an Olympus X-81 fluorescence microscope.

458 **Protein purification**. 10 ml overnight *E. coli* cultures were transferred to 400 ml LB
459 medium supplemented with 100 µg/ml ampicillin or 30 µg/ml kanamycin and grown to
460 OD_{600nm} of 0.8-1.0. Cultures were then incubated at 18°C for 16-18 h after the addition of
461 IPTG at a final concentration of 0.5 mM. Bacterial cells were spun down at 12,000 g and
462 lysed by sonication. The soluble lysates were cleared by spinning at 12,000*g* twice at 4°C
463 for 20 minutes. To purify His_6-tagged proteins, supernatants were incubated with Ni^{2+}-
464 NTA beads for 2 h at 4°C followed by elution with 300 mM imidazole in TBS buffer after
465 washing with 20X bed volumes of TBS buffer containing 20 mM imidazole. Purified
466 proteins were dialyzed in buffer containing TBS, 5% glycerol and 1 mM DTT overnight at
467 4°C. GST-tagged proteins were purified with glutathione beads (Pierce, cat# 16101) for
468 2 h at 4°C followed by elution with elution buffer (50 Mm Tris pH 8.0, 0.4 M NaCl, 50 mM
469 reduced glutathione, 0.1% Triton X-100, 1 mM DTT).

470 **shRNA knockdown of *AMOT* and *AMOTL1***. MISSION shRNA retroviral constructs
471 targeting *AMOT* was purchased from Sigma-Aldrich (Clone ID: NM_133265.1-1628s1c1).
472 To collect viral supernatant, cells were seeded at $2x10^5$ cells/6 cm plate (around 10%
473 confluency). After overnight culture, cells were transfected with the retroviral construct
474 targeting *AMOT* along with two packing plasmids, psPAX2 and pMD2.G. The viral
475 supernatant was collected at day 5 after transfection and was filtered with a 0.45-µm
476 syringe filter. The titer of the produced lentivirus was determined by using Lenti-X Gostix

Plus Titer Kit (Takara, cat# 631281). To generate *AMOT* knockdown cell line, HEK293T cells were seeded at $2x10^5$ cells/10 cm plate (around 10% confluency). Media was removed at day 2 and viral supernatant was added to cover the whole plate (3.5 ml/10 cm plate). Viral supernatant was added every 3 hours for three times. At day 3, media was replaced with fresh media. Cells were selected with media supplemented with puromycin (InvivoGen, cat# ant-pr-1) for a few days and single colonies were selected.

To generate *AMOTL1* knockdown cell line, the pLKO.1-hygro-*AMOTL1*-sh construct was generated by cloning annealed oligos 5'-CCGGTCCGGGCCCATCCTACAAACAACTTTCTCGAGAAAGTT GTTTGTAGGATGGGCTTTTTTGG-3' and 5'-AATTCCAAAAAAGCCCATCCTACAAAC AACTTTCTCGAGAAAGTTGTTTGTAGGATGGGCCCGGA-3' into the pLKO.1-hygro vector. Viral supernatant was generated by transfecting HEK293T cells with the retroviral construct targeting *AMOTL1* along with the packing plasmids, psPAX2 and pMD2.G. The viral supernatant was collected as described above. The *AMOT* knockdown cell line was infected with the viral supernatant as described above and single colonies were selected with media supplemented with hygromycin (Thermo Fisher Scientific, cat#10687010).

Cell-free assays and *in vitro* assays. In the cell-free assays, HEK293T cells expressing Flag-Actin, HA-AMOT, GFP-RavJ, GPF-RavJ$_{C101A}$, HA-LegL1, respectively, were lysed by RIPA buffer without EDTA. Cell lysates were spun down at 12,000 g and the supernatants were collected. Reactions with combined supernatants as indicated were allowed to proceed for 2h at 37°C. the supernatants were then subjected to immunoprecipitation with Flag-antibody coated beads or HA-antibody coated beads as needed.

For *in vitro* assays, HEK293T cells expressing HA-AMOT, Flag-Actin respectively were lysed with RIPA buffer and then subjected to HA-IP or Flag-IP as needed. Proteins were eluted from the corresponding beads using 3XFLAG peptide or HA peptide (Thermo Fisher Scientific). 5 μg His_6-RavJ or His_6-$RavJ_{C101A}$ were added to the *in vitro* assay and the reaction was left in the 37°C incubator for 2 h. The in vitro reaction was then subjected to Flag-IP followed by SDS-PAGE analysis.

Intracellular bacterial growth assay. *L. pneumophila* strains were grown to the post-exponential phase (OD_{600}=3.2-3.8) before infection. Bone marrow-derived mouse macrophages (BMDMs) isolated from female A/J mice as described before[58] were seeded onto 24-well plates and were infected with relevant *L. pneumophila* strains at an MOI of 0.05 at 37°C. Cells were collected at the indicated time points and lysed with 0.02% saponin for half an hour on ice. The bacteria number was determined by enumerating colony-forming unit (CFU) of appropriately diluted saponin-soluble fractions.

LC-MS/MS analysis. Protein bands were digested in-gel with trypsin for protein identification. Peptides were re-suspended in 96.9% water, 3% acetonitrile (ACN), and 0.1% formic acid (FA) at the final concentration of 0.2μg/μl, and 1 μg total peptides (equivalent volume) was analyzed by LC-ESI-MS/MS system using the Dionex UltiMate 3000 RSLC nano System coupled to the Q Exactive™ HF Hybrid Quadrupole-Orbitrap Mass Spectrometer (Thermo Scientific, Waltham, MA) as described previously[65, 66]. The reverse phase peptide separation was accomplished using a trap column (300 μm ID × 5 mm) packed with 5 μm 100 Å PepMap C18 medium, and then separated on a reverse phase column (50-cm long × 75 μm ID) packed with 2 μm 100 Å PepMap C18

522 silica (Thermo Fisher Scientific, Waltham, MA). The column temperature was maintained
523 at 50 °C.

524 Mobile phase solvent A was 0.1% FA in water and solvent B was 0.1% FA in 80%
525 ACN. Loading buffer was 98%/water/2% ACN/0.1% FA. Peptides were separated by
526 loading into the trap column in a loading buffer for 5-min at 5 µL/min flow rate and eluted
527 from the analytical column at a flow rate of 150 nL/min using a 130-min LC gradient as
528 follows: linear gradient of 5.1 to 27% of solvent B in 80 min, 27-45% in next 20 min, 45-
529 100% of B in next 5 min at which point the gradient was held at 100% of B for 7 min before
530 reverting back to 2% of B at 112 min, and hold at 2% of B for next 18 min for equilibration.
531 The mass spectrometer was operated in positive ion and standard data-dependent
532 acquisition mode with Advanced Peak Detection function activated for the top 20n. The
533 fragmentation of precursor ion was accomplished by stepped normalized collision energy
534 setting of 27%. The resolution of Orbitrap mass analyzer was set to 120,000 and 15,000
535 for MS1 and MS2, respectively. The full scan MS1 spectra were collected in the mass
536 range of 350-1,600 m/z, with an isolation window of 1.2m/z and a fixed first mass of 100
537 m/z for MS2. The spray voltage was set at 2 and Automatic Gain Control (AGC) target of
538 4e5 for MS1 and 5e4 for MS2, respectively.

539 For protein identification, the raw data were processed with the software
540 MaxQuant[67] (version 1.6.3.3) against *Homo sapiens* database downloaded from the
541 UniProt (www.uniprot.org). The following parameters were edited for the searches:
542 precursor mass tolerance of 10 ppm; enzyme specificity of trypsin enzyme allowing up to
543 2 missed cleavages; oxidation of methionine (M) as a variable modification and
544 carbamidomethylation of cysteine (C) as a fixed modification. False discovery rate (FDR)

of peptide spectral match (PSM) and protein identification was set to 0.01. The unique plus razor peptides (non-redundant, non-unique peptides assigned to the protein group with most other peptides) were used for peptide quantitation. LFQ intensity values were used for relative protein abundance measurement. Only proteins detected with at least one unique peptide and MS/MS ≥2 (spectral counts) were considered as true identification and used for downstream analysis.

Materials Availability Statement: All unique constructs and cell lines described in this article are available upon reasonable request from academic researchers. Please contact the corresponding author at luoz@purdue.edu for request of any materials.

556 **Acknowledgements:** We thank Drs. Qing Deng, Matthew Olson and Chittaranjan Das
557 (Purdue University) for helpful suggestions. We thank members of the Luo laboratory for
558 helpful discussion. We also thank Dr. Uma K. Aryal from Purdue University and Dr.
559 Jonathan Trinidad from the laboratory for Biological Mass Spectrometry at Indiana
560 University for assistance in mass spectrometry analysis.

561

References

1. Vogel JP, Andrews HL, Wong SK, Isberg RR. Conjugative transfer by the virulence system of Legionella pneumophila. Science. 1998;279(5352):873-6. doi: 10.1126/science.279.5352.873. PubMed PMID: 9452389.
2. Qiu J, Luo ZQ. Legionella and Coxiella effectors: strength in diversity and activity. Nat Rev Microbiol. 2017;15(10):591-605. Epub 20170717. doi: 10.1038/nrmicro.2017.67. PubMed PMID: 28713154.
3. Qiu J, Luo ZQ. Hijacking of the Host Ubiquitin Network by. Front Cell Infect Microbiol. 2017;7:487. Epub 20171205. doi: 10.3389/fcimb.2017.00487. PubMed PMID: 29376029; PubMed Central PMCID: PMCPMC5770618.
4. Isberg RR, O'Connor TJ, Heidtman M. The Legionella pneumophila replication vacuole: making a cosy niche inside host cells. Nat Rev Microbiol. 2009;7(1):13-24. Epub 20081117. doi: 10.1038/nrmicro1967. PubMed PMID: 19011659; PubMed Central PMCID: PMCPMC2631402.
5. Zhu W, Banga S, Tan Y, Zheng C, Stephenson R, Gately J, et al. Comprehensive identification of protein substrates of the Dot/Icm type IV transporter of Legionella pneumophila. PLoS One. 2011;6(3):e17638. Epub 20110309. doi: 10.1371/journal.pone.0017638. PubMed PMID: 21408005; PubMed Central PMCID: PMCPMC3052360.
6. Huang L, Boyd D, Amyot WM, Hempstead AD, Luo ZQ, O'Connor TJ, et al. The E Block motif is associated with Legionella pneumophila translocated substrates. Cell Microbiol. 2011;13(2):227-45. Epub 20101103. doi: 10.1111/j.1462-5822.2010.01531.x. PubMed PMID: 20880356; PubMed Central PMCID: PMCPMC3096851.
7. Pollard TD, Cooper JA. Actin, a central player in cell shape and movement. Science. 2009;326(5957):1208-12. doi: 10.1126/science.1175862. PubMed PMID: 19965462; PubMed Central PMCID: PMCPMC3677050.
8. Richard JF, Petit L, Gibert M, Marvaud JC, Bouchaud C, Popoff MR. Bacterial toxins modifying the actin cytoskeleton. Int Microbiol. 1999;2(3):185-94. PubMed PMID: 10943412.
9. Ono S. A plague of actin disassembly. J Biol Chem. 2017;292(19):8101-2. doi: 10.1074/jbc.H116.757971. PubMed PMID: 28500241; PubMed Central PMCID: PMCPMC5427285.
10. Galan JE, Zhou D. Striking a balance: modulation of the actin cytoskeleton by Salmonella. Proc Natl Acad Sci U S A. 2000;97(16):8754-61. doi: 10.1073/pnas.97.16.8754. PubMed PMID: 10922031; PubMed Central PMCID: PMCPMC34008.
11. Liu Y, Zhu W, Tan Y, Nakayasu ES, Staiger CJ, Luo ZQ. A Legionella Effector Disrupts Host Cytoskeletal Structure by Cleaving Actin. PLoS Pathog. 2017;13(1):e1006186. Epub 20170127. doi: 10.1371/journal.ppat.1006186. PubMed PMID: 28129393; PubMed Central PMCID: PMCPMC5298343.
12. Michard C, Sperandio D, Baïlo N, Pizarro-Cerdá J, LeClaire L, Chadeau-Argaud E, et al. The Legionella Kinase LegK2 Targets the ARP2/3 Complex To Inhibit Actin Nucleation on Phagosomes and Allow Bacterial Evasion of the Late Endocytic Pathway. mBio. 2015;6(3):e00354-15. Epub 20150505. doi: 10.1128/mBio.00354-15. PubMed PMID: 25944859; PubMed Central PMCID: PMCPMC4436068.

13. Guo Z, Stephenson R, Qiu J, Zheng S, Luo ZQ. A Legionella effector modulates host cytoskeletal structure by inhibiting actin polymerization. Microbes Infect. 2014;16(3):225-36. Epub 20131126. doi: 10.1016/j.micinf.2013.11.007. PubMed PMID: 24286927; PubMed Central PMCID: PMCPMC3965633.
14. Franco IS, Shohdy N, Shuman HA. The Legionella pneumophila effector VipA is an actin nucleator that alters host cell organelle trafficking. PLoS Pathog. 2012;8(2):e1002546. Epub 20120223. doi: 10.1371/journal.ppat.1002546. PubMed PMID: 22383880; PubMed Central PMCID: PMCPMC3285593.
15. Chambers KA, Scheck RA. Bacterial virulence mediated by orthogonal post-translational modification. Nat Chem Biol. 2020;16(10):1043-51. Epub 20200917. doi: 10.1038/s41589-020-0638-2. PubMed PMID: 32943788.
16. Mukherjee S, Liu X, Arasaki K, McDonough J, Galán JE, Roy CR. Modulation of Rab GTPase function by a protein phosphocholine transferase. Nature. 2011;477(7362):103-6. Epub 20110807. doi: 10.1038/nature10335. PubMed PMID: 21822290; PubMed Central PMCID: PMCPMC3206611.
17. Tan Y, Arnold RJ, Luo ZQ. Legionella pneumophila regulates the small GTPase Rab1 activity by reversible phosphorylcholination. Proc Natl Acad Sci U S A. 2011;108(52):21212-7. Epub 20111207. doi: 10.1073/pnas.1114023109. PubMed PMID: 22158903; PubMed Central PMCID: PMCPMC3248503.
18. Müller MP, Peters H, Blümer J, Blankenfeldt W, Goody RS, Itzen A. The Legionella effector protein DrrA AMPylates the membrane traffic regulator Rab1b. Science. 2010;329(5994):946-9. Epub 20100722. doi: 10.1126/science.1192276. PubMed PMID: 20651120.
19. Lee PC, Machner MP. The Legionella Effector Kinase LegK7 Hijacks the Host Hippo Pathway to Promote Infection. Cell Host Microbe. 2018;24(3):429-38.e6. doi: 10.1016/j.chom.2018.08.004. PubMed PMID: 30212651; PubMed Central PMCID: PMCPMC7343393.
20. Qiu J, Sheedlo MJ, Yu K, Tan Y, Nakayasu ES, Das C, et al. Ubiquitination independent of E1 and E2 enzymes by bacterial effectors. Nature. 2016;533(7601):120-4. Epub 20160406. doi: 10.1038/nature17657. PubMed PMID: 27049943; PubMed Central PMCID: PMCPMC4905768.
21. Black MH, Osinski A, Park GJ, Gradowski M, Servage KA, Pawłowski K, et al. A Legionella effector ADP-ribosyltransferase inactivates glutamate dehydrogenase. J Biol Chem. 2021;296:100301. Epub 20210118. doi: 10.1016/j.jbc.2021.100301. PubMed PMID: 33476647; PubMed Central PMCID: PMCPMC7949102.
22. Fu J, Zhou M, Gritsenko MA, Nakayasu ES, Song L, Luo ZQ. modulates host energy metabolism by ADP-ribosylation of ADP/ATP translocases. Elife. 2022;11. Epub 20220127. doi: 10.7554/eLife.73611. PubMed PMID: 35084332; PubMed Central PMCID: PMCPMC8820735.
23. Gan N, Nakayasu ES, Hollenbeck PJ, Luo ZQ. Legionella pneumophila inhibits immune signalling via MavC-mediated transglutaminase-induced ubiquitination of UBE2N. Nat Microbiol. 2019;4(1):134-43. Epub 20181112. doi: 10.1038/s41564-018-0282-8. PubMed PMID: 30420781; PubMed Central PMCID: PMCPMC6294664.
24. Lorand L, Graham RM. Transglutaminases: crosslinking enzymes with pleiotropic functions. Nat Rev Mol Cell Biol. 2003;4(2):140-56. doi: 10.1038/nrm1014. PubMed PMID: 12563291.

25. Nimchuk ZL, Fisher EJ, Desveaux D, Chang JH, Dangl JL. The HopX (AvrPphE) family of Pseudomonas syringae type III effectors require a catalytic triad and a novel N-terminal domain for function. Mol Plant Microbe Interact. 2007;20(4):346-57. doi: 10.1094/MPMI-20-4-0346. PubMed PMID: 17427805.
26. Zhang L, Krachler AM, Broberg CA, Li Y, Mirzaei H, Gilpin CJ, et al. Type III effector VopC mediates invasion for Vibrio species. Cell Rep. 2012;1(5):453-60. Epub 20120503. doi: 10.1016/j.celrep.2012.04.004. PubMed PMID: 22787576; PubMed Central PMCID: PMCPMC3392014.
27. Urbanus ML, Quaile AT, Stogios PJ, Morar M, Rao C, Di Leo R, et al. Diverse mechanisms of metaeffector activity in an intracellular bacterial pathogen, Legionella pneumophila. Mol Syst Biol. 2016;12(12):893. Epub 20161216. doi: 10.15252/msb.20167381. PubMed PMID: 27986836; PubMed Central PMCID: PMCPMC5199130.
28. Huang T, Zhou Y, Zhang J, Cheng ASL, Yu J, To KF, et al. The physiological role of Motin family and its dysregulation in tumorigenesis. J Transl Med. 2018;16(1):98. Epub 20180412. doi: 10.1186/s12967-018-1466-y. PubMed PMID: 29650031; PubMed Central PMCID: PMCPMC5898069.
29. Bratt A, Wilson WJ, Troyanovsky B, Aase K, Kessler R, Van Meir EG, et al. Angiomotin belongs to a novel protein family with conserved coiled-coil and PDZ binding domains. Gene. 2002;298(1):69-77. doi: 10.1016/s0378-1119(02)00928-9. PubMed PMID: 12406577.
30. Zhao B, Li L, Lu Q, Wang LH, Liu CY, Lei Q, et al. Angiomotin is a novel Hippo pathway component that inhibits YAP oncoprotein. Genes Dev. 2011;25(1):51-63. doi: 10.1101/gad.2000111. PubMed PMID: 21205866; PubMed Central PMCID: PMCPMC3012936.
31. McGough A, Pope B, Chiu W, Weeds A. Cofilin changes the twist of F-actin: implications for actin filament dynamics and cellular function. J Cell Biol. 1997;138(4):771-81. doi: 10.1083/jcb.138.4.771. PubMed PMID: 9265645; PubMed Central PMCID: PMCPMC2138052.
32. Schutt CE, Myslik JC, Rozycki MD, Goonesekere NC, Lindberg U. The structure of crystalline profilin-beta-actin. Nature. 1993;365(6449):810-6. doi: 10.1038/365810a0. PubMed PMID: 8413665.
33. Ezezika OC, Younger NS, Lu J, Kaiser DA, Corbin ZA, Nolen BJ, et al. Incompatibility with formin Cdc12p prevents human profilin from substituting for fission yeast profilin: insights from crystal structures of fission yeast profilin. J Biol Chem. 2009;284(4):2088-97. Epub 20081120. doi: 10.1074/jbc.M807073200. PubMed PMID: 19028693; PubMed Central PMCID: PMCPMC2629104.
34. Pfaendtner J, De La Cruz EM, Voth GA. Actin filament remodeling by actin depolymerization factor/cofilin. Proc Natl Acad Sci U S A. 2010;107(16):7299-304. Epub 20100405. doi: 10.1073/pnas.0911675107. PubMed PMID: 20368459; PubMed Central PMCID: PMCPMC2867716.
35. Revenu C, Athman R, Robine S, Louvard D. The co-workers of actin filaments: from cell structures to signals. Nat Rev Mol Cell Biol. 2004;5(8):635-46. doi: 10.1038/nrm1437. PubMed PMID: 15366707.
36. Colonne PM, Winchell CG, Voth DE. Hijacking Host Cell Highways: Manipulation of the Host Actin Cytoskeleton by Obligate Intracellular Bacterial Pathogens. Front Cell

699 Infect Microbiol. 2016;6:107. Epub 20160922. doi: 10.3389/fcimb.2016.00107. PubMed
700 PMID: 27713866; PubMed Central PMCID: PMCPMC5031698.
701 37. Meconi S, Jacomo V, Boquet P, Raoult D, Mege JL, Capo C. Coxiella burnetii
702 induces reorganization of the actin cytoskeleton in human monocytes. Infect Immun.
703 1998;66(11):5527-33. doi: 10.1128/IAI.66.11.5527-5533.1998. PubMed PMID: 9784567;
704 PubMed Central PMCID: PMCPMC108693.
705 38. Aguilera M, Salinas R, Rosales E, Carminati S, Colombo MI, Berón W. Actin
706 dynamics and Rho GTPases regulate the size and formation of parasitophorous vacuoles
707 containing Coxiella burnetii. Infect Immun. 2009;77(10):4609-20. Epub 20090727. doi:
708 10.1128/IAI.00301-09. PubMed PMID: 19635823; PubMed Central PMCID:
709 PMCPMC2747940.
710 39. Campbell S, Richmond SJ, Yates PS. The effect of Chlamydia trachomatis
711 infection on the host cell cytoskeleton and membrane compartments. J Gen Microbiol.
712 1989;135(9):2379-86. doi: 10.1099/00221287-135-9-2379. PubMed PMID: 2483409.
713 40. Kumar Y, Valdivia RH. Actin and intermediate filaments stabilize the Chlamydia
714 trachomatis vacuole by forming dynamic structural scaffolds. Cell Host Microbe.
715 2008;4(2):159-69. doi: 10.1016/j.chom.2008.05.018. PubMed PMID: 18692775; PubMed
716 Central PMCID: PMCPMC2605408.
717 41. Gouin E, Egile C, Dehoux P, Villiers V, Adams J, Gertler F, et al. The RickA protein
718 of Rickettsia conorii activates the Arp2/3 complex. Nature. 2004;427(6973):457-61. doi:
719 10.1038/nature02318. PubMed PMID: 14749835.
720 42. Jeng RL, Goley ED, D'Alessio JA, Chaga OY, Svitkina TM, Borisy GG, et al. A
721 Rickettsia WASP-like protein activates the Arp2/3 complex and mediates actin-based
722 motility. Cell Microbiol. 2004;6(8):761-9. doi: 10.1111/j.1462-5822.2004.00402.x.
723 PubMed PMID: 15236643.
724 43. Oda T, Iwasa M, Aihara T, Maéda Y, Narita A. The nature of the globular- to
725 fibrous-actin transition. Nature. 2009;457(7228):441-5. doi: 10.1038/nature07685.
726 PubMed PMID: 19158791.
727 44. Martinez-Quiles N, Rohatgi R, Antón IM, Medina M, Saville SP, Miki H, et al. WIP
728 regulates N-WASP-mediated actin polymerization and filopodium formation. Nat Cell Biol.
729 2001;3(5):484-91. doi: 10.1038/35074551. PubMed PMID: 11331876.
730 45. Kühn S, Mannherz HG. Actin: Structure, Function, Dynamics, and Interactions with
731 Bacterial Toxins. Curr Top Microbiol Immunol. 2017;399:1-34. doi: 10.1007/82_2016_45.
732 PubMed PMID: 27848038.
733 46. Horwitz MA. The Legionnaires' disease bacterium (Legionella pneumophila)
734 inhibits phagosome-lysosome fusion in human monocytes. J Exp Med.
735 1983;158(6):2108-26. doi: 10.1084/jem.158.6.2108. PubMed PMID: 6644240; PubMed
736 Central PMCID: PMCPMC2187157.
737 47. Derré I, Isberg RR. Legionella pneumophila replication vacuole formation involves
738 rapid recruitment of proteins of the early secretory system. Infect Immun.
739 2004;72(5):3048-53. doi: 10.1128/IAI.72.5.3048-3053.2004. PubMed PMID: 15102819;
740 PubMed Central PMCID: PMCPMC387905.
741 48. Swanson MS, Isberg RR. Association of Legionella pneumophila with the
742 macrophage endoplasmic reticulum. Infect Immun. 1995;63(9):3609-20. doi:
743 10.1128/iai.63.9.3609-3620.1995. PubMed PMID: 7642298; PubMed Central PMCID:
744 PMCPMC173501.

745 49. Kagan JC, Roy CR. Legionella phagosomes intercept vesicular traffic from
746 endoplasmic reticulum exit sites. Nat Cell Biol. 2002;4(12):945-54. doi: 10.1038/ncb883.
747 PubMed PMID: 12447391.
748 50. Shin S, Roy CR. Host cell processes that influence the intracellular survival of
749 Legionella pneumophila. Cell Microbiol. 2008;10(6):1209-20. Epub 20080317. doi:
750 10.1111/j.1462-5822.2008.01145.x. PubMed PMID: 18363881.
751 51. Heidtman M, Chen EJ, Moy MY, Isberg RR. Large-scale identification of Legionella
752 pneumophila Dot/Icm substrates that modulate host cell vesicle trafficking pathways. Cell
753 Microbiol. 2009;11(2):230-48. Epub 20081030. doi: 10.1111/j.1462-5822.2008.01249.x.
754 PubMed PMID: 19016775; PubMed Central PMCID: PMCPMC2744955.
755 52. Iyer S, Das C. The unity of opposites: Strategic interplay between bacterial
756 effectors to regulate cellular homeostasis. J Biol Chem. 2021;297(6):101340. Epub
757 20211023. doi: 10.1016/j.jbc.2021.101340. PubMed PMID: 34695417; PubMed Central
758 PMCID: PMCPMC8605245.
759 53. Hehnly H, Stamnes M. Regulating cytoskeleton-based vesicle motility. FEBS Lett.
760 2007;581(11):2112-8. Epub 20070220. doi: 10.1016/j.febslet.2007.01.094. PubMed
761 PMID: 17335816; PubMed Central PMCID: PMCPMC1974873.
762 54. Kee AJ, Bryce NS, Yang L, Polishchuk E, Schevzov G, Weigert R, et al. ER/Golgi
763 trafficking is facilitated by unbranched actin filaments containing Tpm4.2. Cytoskeleton
764 (Hoboken). 2017;74(10):379-89. Epub 20170831. doi: 10.1002/cm.21405. PubMed
765 PMID: 28834398; PubMed Central PMCID: PMCPMC7971414.
766 55. Berger KH, Isberg RR. Two distinct defects in intracellular growth complemented
767 by a single genetic locus in Legionella pneumophila. Mol Microbiol. 1993;7(1):7-19. doi:
768 10.1111/j.1365-2958.1993.tb01092.x. PubMed PMID: 8382332.
769 56. Berger KH, Merriam JJ, Isberg RR. Altered intracellular targeting properties
770 associated with mutations in the Legionella pneumophila dotA gene. Mol Microbiol.
771 1994;14(4):809-22. doi: 10.1111/j.1365-2958.1994.tb01317.x. PubMed PMID: 7891566.
772 57. Luo ZQ, Isberg RR. Multiple substrates of the Legionella pneumophila Dot/Icm
773 system identified by interbacterial protein transfer. Proc Natl Acad Sci U S A.
774 2004;101(3):841-6. Epub 20040108. doi: 10.1073/pnas.0304916101. PubMed PMID:
775 14715899; PubMed Central PMCID: PMCPMC321768.
776 58. Conover GM, Derré I, Vogel JP, Isberg RR. The Legionella pneumophila LidA
777 protein: a translocated substrate of the Dot/Icm system associated with maintenance of
778 bacterial integrity. Mol Microbiol. 2003;48(2):305-21. doi: 10.1046/j.1365-
779 2958.2003.03400.x. PubMed PMID: 12675793.
780 59. Luo ZQ, Farrand SK. Signal-dependent DNA binding and functional domains of
781 the quorum-sensing activator TraR as identified by repressor activity. Proc Natl Acad Sci
782 U S A. 1999;96(16):9009-14. doi: 10.1073/pnas.96.16.9009. PubMed PMID: 10430886;
783 PubMed Central PMCID: PMCPMC17723.
784 60. McCloskey A, Perri K, Chen T, Han A, Luo ZQ. The metaeffector MesI regulates
785 the activity of the Legionella effector SidI through direct protein-protein interactions.
786 Microbes Infect. 2021;23(4-5):104794. Epub 20210208. doi:
787 10.1016/j.micinf.2021.104794. PubMed PMID: 33571674; PubMed Central PMCID:
788 PMCPMC9406241.
789 61. Xu L, Shen X, Bryan A, Banga S, Swanson MS, Luo ZQ. Inhibition of host vacuolar
790 H+-ATPase activity by a Legionella pneumophila effector. PLoS Pathog.

2010;6(3):e1000822. Epub 20100319. doi: 10.1371/journal.ppat.1000822. PubMed PMID: 20333253; PubMed Central PMCID: PMCPMC2841630.

62. Sheedlo MJ, Qiu J, Tan Y, Paul LN, Luo ZQ, Das C. Structural basis of substrate recognition by a bacterial deubiquitinase important for dynamics of phagosome ubiquitination. Proc Natl Acad Sci U S A. 2015;112(49):15090-5. Epub 20151123. doi: 10.1073/pnas.1514568112. PubMed PMID: 26598703; PubMed Central PMCID: PMCPMC4679006.

63. Wang SH, Wang A, Liu PP, Zhang WY, Du J, Xu S, et al. Divergent Pathogenic Properties of Circulating Coxsackievirus A6 Associated with Emerging Hand, Foot, and Mouth Disease. J Virol. 2018;92(11). Epub 20180514. doi: 10.1128/JVI.00303-18. PubMed PMID: 29563294; PubMed Central PMCID: PMCPMC5952127.

64. Hubber A, Arasaki K, Nakatsu F, Hardiman C, Lambright D, De Camilli P, et al. The machinery at endoplasmic reticulum-plasma membrane contact sites contributes to spatial regulation of multiple Legionella effector proteins. PLoS Pathog. 2014;10(7):e1004222. Epub 20140703. doi: 10.1371/journal.ppat.1004222. PubMed PMID: 24992562; PubMed Central PMCID: PMCPMC4081824.

65. Connelly KE, Hedrick V, Paschoal Sobreira TJ, Dykhuizen EC, Aryal UK. Analysis of Human Nuclear Protein Complexes by Quantitative Mass Spectrometry Profiling. Proteomics. 2018;18(11):e1700427. Epub 20180504. doi: 10.1002/pmic.201700427. PubMed PMID: 29655301; PubMed Central PMCID: PMCPMC6387628.

66. Mohallem R, Aryal UK. Regulators of TNFα mediated insulin resistance elucidated by quantitative proteomics. Sci Rep. 2020;10(1):20878. Epub 20201130. doi: 10.1038/s41598-020-77914-1. PubMed PMID: 33257747; PubMed Central PMCID: PMCPMC7705713.

67. Cox J, Mann M. MaxQuant enables high peptide identification rates, individualized p.p.b.-range mass accuracies and proteome-wide protein quantification. Nat Biotechnol. 2008;26(12):1367-72. Epub 20081130. doi: 10.1038/nbt.1511. PubMed PMID: 19029910.